Landscape and Urban Planning 238 (2023) 104831

Contents lists available at ScienceDirect

Landscape and Urban Planning

journal homepage: www.elsevier.com/locate/landurbplan

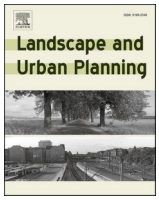

Mapping urban heat islands and heat-related risk during heat waves from a climate justice perspective: A case study in the municipality of Padua (Italy) for inclusive adaptation policies

Salvatore Eugenio Pappalardo [a,c,*], Carlo Zanetti [b,c], Valeria Todeschi [a]

[a] Advanced Master GIScience and UAV, Department of Civil, Environmental and Architectural Engineering (ICEA), University of Padua, 35100 Padua, Italy
[b] University of Padua, Department of Civil Environmental and Architectural Engineering, Italy
[c] Laboratory GIScience and Drones for Good, Department of Civil, Environmental and Architectural Engineering, University of Padua, Italy

HIGHLIGHTS

- In summer 2022 three extreme heatwaves hit Padua, with maximum temperatures of 35.1 °C, 36.1 °C, and 35.8 °C.
- Magnitude of urban heat islands reached 3–8 °C temperature anomaly, with an increase of 0.3 °C every 10% of soil sealing.
- The highest climate risk is found on the spatial compresence of elderly, migrants, children and households at low income.
- The GIS-based climate risk methodology provides essential insights to support inclusive and more just adaptation plannings.

ARTICLE INFO

Keywords:
Climate Justice
Urban heat islands
Heat waves
Inclusive climate adaptation policies
Urban resilience
Italy

ABSTRACT

Climate change has led to a dramatic increase in extreme events worldwide. Predictions for a + 1.5 °C world indicate that 13.8% of the global population will be exposed to heat waves (HWs), a proportion rising to 36.9% in a + 2 °C scenario. At present, about 9.6 M people in the EU and UK are exposed to extreme heat every year. Overheating has various impacts on cities, including urban infrastructure failures and changes in ecological processes. However, scarce attention is currently paid to the distribution of HWs impacts and the differential vulnerabilities of different social groups, raising the issue of climate justice in cities. HWs directly impact the health of the most vulnerable social groups resulting in an increase in mortality and morbidity rates. This research focuses on the city of Padua (Italy) as a pilot study to assess the effects of urban HWs and heat islands (UHI) combined. By framing the unequal spatial distribution of socially vulnerable groups, this study aims to i) provide a replicable spatially explicit open-access methodology to assess the heat-related risk of UHI; ii) propose the first climate justice heat-related risk index to be adopted in inclusive and just adaptation plans. Specifically, it aims to i) identify HWs and map critical hotspots during summer 2022 at suburban scale; ii) assess the spatial correlations among impervious areas and UHI; iii) map the climate risk to vulnerable social groups; and iv) propose a global climate justice risk index for all the vulnerable groups considered. Images from Landsat 8–9 were processed, and territorial data were acquired from public databases. It was found that three extreme HWs hit Padua in summer 2022, on 2–7 June, 21–23 July, and 4–8 August, when maximum temperatures were 35.1 °C, 36.1 °C, and 35.8 °C, respectively. The intensity and magnitude of UHIs were considerable, with land surface temperatures of 33.8 °C on average ($\sigma = 1.7$, min = 27.9, max = 41.4). UHI intensity reached 5–8 °C of difference with rural contexts, mainly in strongly urbanized sectors. Ordinary least squares regression indicated a positive correlation with impervious surfaces, with a β coefficient showing an average increase of 0.3 °C per 10% of soil sealing. Six different hotspots were identified both in industrial areas and within the city centre. However, the integrated climate risk analyses highlight that most critical areas are in sectors where there is a large number of the elderly, migrants, children, and low-income households. Our findings reveal the need for urgent heat island mitigation measures and that the distributive dimension of climate justice should be respected in adaptation planning.

* Corresponding author.
E-mail address: salvatore.pappalardo@unipd.it (S. Eugenio Pappalardo).

https://doi.org/10.1016/j.landurbplan.2023.104831
Received 8 January 2023; Received in revised form 15 May 2023; Accepted 11 June 2023
Available online 3 July 2023

1. Introduction

1.1. Climate extremes: Heat waves and heat islands in urban areas

In spring and summer 2022, the effects of climate change made themselves felt in the daily life of hundreds of millions of people in the northern hemisphere as well as the global mainstream media (Andersson & Faulkner, 2022; Fears & Eger, 2022; Gualtieri & Sundby, 2022). A sequence of heatwaves (HWs) of unprecedented magnitude and intensity hit highly densely populated areas in Asia, North America, and Europe, giving a new picture of what the direct and indirect impacts of climate change on these territories look like, especially in urban areas (World Meteorological Organization (WMO, 2022a; WMO, 2022c; WMO, 2022d)). According to the Intergovernmental Panel on Climate Change (IPCC), it is "virtually certain" (99–100% probability) that HWs will increase across most land regions in frequency, magnitude, and duration, and there is "high confidence" that they are driven by human activities (IPCC, 2021). Therefore, due to a combination of climate change effects and urbanization processes (e.g., expansion and densification), HWs have become a crucial challenge for urban development.

Predictions for a world at 1.5 °C highlighted that 13.8% of the global population will be exposed to extreme HWs, while in a 2 °C warming scenario this estimation rises to 36.9% (Dosio et al., 2018). Due to these increases in intensity and magnitude and the consequent impacts on ecosystems and societies, the WMO called climate extremes the day-to-day "face" of climate change (WMO, 2022b).

Europe, the second densely populated continent (72.5 inhabitants/km^2) after Asia (95 inhabitants/km^2), is characterized by wide urbanized areas, which house 72% of the total population (World Bank, 2023). It has experienced a large increase in extreme HWs since the "deadly summer" of 2003, which caused ~ 70,000 estimated excess deaths (Robine et al., 2008) and was followed by severe events in Finland (2018), Russia (2010), and Greece (2012) (Porfiriev, 2014; Paravantis et al., 2017; Ruuhela et al., 2020). Excess mortality in Europe reached + 16% during July 2022 compared to average mortality in the same month in the period 2016–2019, with peaks of + 25–37% in Mediterranean countries (EUROSTAT, 2022). Furthermore, changes in atmospheric dynamics have made Europe a crucial HW hotspot: the incidence of HWs will accelerate three to four times faster than the rate experienced in the northern mid-latitudes over the last 42 years (Rousi et al., 2022).

Urban areas are vulnerable to heat islands due to their typical land use land cover (LULC), population density, infrastructure systems, assets, and economic activities. The combination of such factors contributes to amplify the effects of extreme weather events, jeopardizing the health of urban dwellers. In fact, although urban areas only cover 3% of the Earth's land surface, they are home to >50% of the world's population and contribute up to 70% of global greenhouse gases emitted while using about 75% of world resources (Yensukho et al., 2022). As such, cities are crucial hotspots where the challenges of climate change will be felt and the effects of urban heat islands (UHIs) must be mitigated. In fact, a global-scale study of 3-day land surface temperature (LST) analyses undertaken over an 18-year period (2003–2020) demonstrated that urban heat increased twofold over that time, with local urban thermal anomalies being >10 °C higher (Mentaschi et al., 2022). Meanwhile, analyses carried out by Guerreiro et al. (2018) based on CMIP5 models for the RCP8.5 scenarios indicated that an increase in the number of HW days and maximum HW temperature is expected in all 571 European cities analyzed in the study, especially in southern and central Europe. Due to the strongly anthropized land cover, mainly represented by impervious surfaces with low albedo as well as a low ratio of build-up to vegetation land cover, the effects of UHI are amplified in the urban context. Studies at urban scale on the cities of Geneve and Paris, based on the use of Land Surface Temperature (LST) derived from Landsat 8 satellite, confirmed significant positive correlation among LST and impervious surface density (Ge et al., 2020).

Moreover, the effect of urban form and morphology is paramount. As reported in different studies based on computational fluid dynamics and neural networks, such factors play a crucial role in influencing urban micro-climate by amplifying extreme conditions (Javanroodi et al., 2022; Mohammad and Javanroodi, 2022; Javanroodi et al., 2021). Consequently, urban areas are generally warmer than the surrounding rural areas as a result of a number of factors that modulate the urban climate and, therefore, form the so-called UHI phenomenon (Oke, 1973). In fact, urbanization processes have led to changes in the physical environment, mainly through LULC changes, which contribute to significant alterations of the urban climate. It has been demonstrated that HWs have positive feedback on UHI, with intensification of magnitude during the event (Founda & Santamouris, 2017).

1.2. Climate justice in the city: Spatial injustice and unequal impacts of heat waves on urban populations

Climate extremes such as HWs and UHIs have direct and indirect impacts locally by affecting societies and economies as well as the remaining anthropized urban ecosystems which still provide essential goods and services to city dwellers. As widely documented, there is strong evidence that HWs have direct impacts on human health, resulting in a significant increase of mortality and morbidity (Nitschke et al., 2011; Mitchell et al., 2016; Romanello et al., 2021). In fact, very hot days on which the temperature exceeds 35 °C (Espírito Santo et al., 2014) together with tropical nights (minimum daily temperature > 20 °C) increase the risk of different cardio-respiratory diseases and other heat-related health issues to city dwellers (Singh et al., 2020). During HWs, tropical nights and hot nights have a particularly important impact on human health as they contribute intensely to thermal discomfort by affecting the human thermoregulatory system and thus preventing nocturnal rest. A recent study performed on 11 European cities found that tropical nights and hot nights are strongly associated with cause-specific fatalities (Royé et al., 2021).

Across the EU and UK combined about 9.6 M people are currently exposed to extreme HWs every year. Naumann et al. (2020) estimated that, under different global warming scenarios, this number will drastically increase, assuming no population growth, to 107.8 M for 1.5 °C (+1121%), 176 M for 2.0 °C (+1932%), and 307 M for 3.0 °C (+3193%). In the last of these scenarios, about half of the European population would be at heat-related risk if no adaptation measures are taken.

As widely documented, the first direct impacts of HWs are on the health of the most fragile segments of societies, including vulnerable social groups such as the elderly (age > 65 years), children (age < 5 years), residents of low-income households, migrants, women, and disadvantaged people, resulting in increased mortality and morbidity rates (Kovats et al., 2004; Morabito et al., 2015; Otto et al., 2017; Nayak et al., 2018). Moreover, psychological impacts on humans are reported during HWs, resulting in an increase of mental health issues and aggressive behavior (Obradovich et al., 2018; Palinkas & Wong, 2020; He et al., 2022). In fact, UHI intensity (UHII) is not equally distributed across the urban space, resulting in highly differentiated impacts on the territory. This phenomenon might exacerbate and polarize existing social inequalities within the urban territory by increasing the gap in the rights to health and raising the issue of justice in regard to both the impacts and the mitigation strategies to be adopted to address climate change (Sanchez-Guevara et al., 2019; Mitchell et al., 2021; Amado, 2022). Only recently, some pioneering research is considering the importance of include the issue of justice and equalities related both to climate change impacts and adaptation planning. In fact, recent scientific and public debates on climate change underscore that it is important for climate adaptation planning to include social aspects related to rights and justice along with physical, economic, and engineering approaches (Gardiner, 2011). In this context, it is thus important that urban planning and management consider inequality, marginalization, and social exclusion alongside vulnerability caused by climate change in order to pursue justice and equity. In fact, only recently the issue of

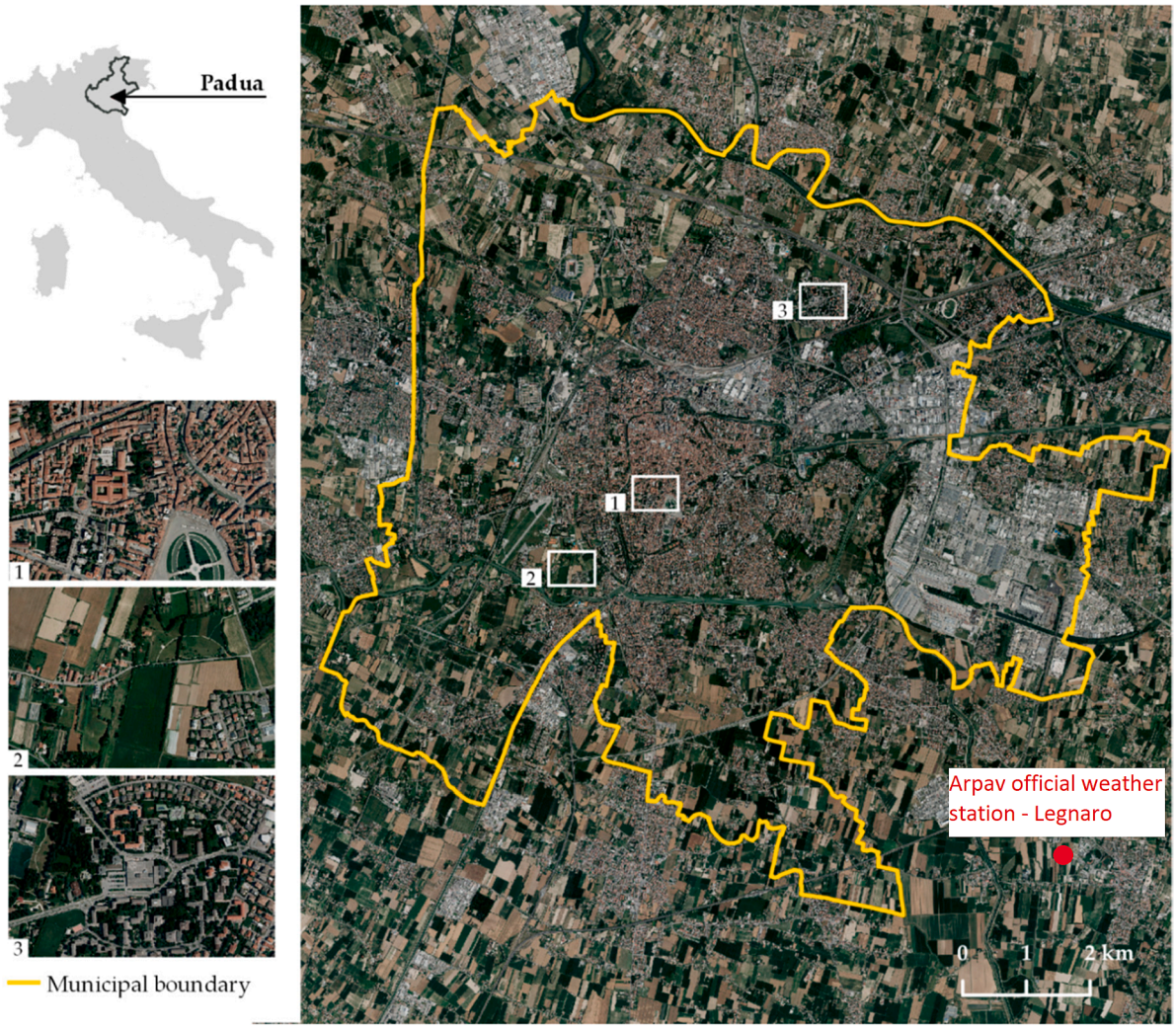

Fig. 1. The city of Padua (93 km^2): Geographic location and urban fabric: 1. Urban, 2. Rural, 3. Mixed.

climate justice was, for the first time, officially recognized both by international climate diplomacy (UNFCCC, 2021) and the IPCC (2022) as a crucial element in understanding how climate change can have spatially and socially differentiated, unequal, and asymmetrical impacts on a territory (Sultana, 2022). Urban heat poses a serious threat to many dimensions of human society, necessitating urgent actions and policies to develop effective adaptation strategies. Overheating might lead to urban infrastructure failures, with loss of water and power as well impacts on energy consumption. In fact, during HWs energy demand for home cooling may cause blackouts and triggers a positive feedback loop (Stone et al., 2021). Increased energy use leads to higher greenhouse gas emissions, creating a trade-off between adapting to extreme heat and mitigating climate change (Colelli et al., 2022). Moreover, HWs might impacts on ecological processes of urban ecosystems, causing relevant changes in carbon sequestration and, therefore, turning urban vegetation from carbon sinks to carbon sources as well as wildfire and damage on agriculture (Ciais et al., 2005; Wang et al. 2021).

1.3. Aims of the study

Our study frames the issue of incorporating a climate justice dimension into more inclusive climate-resilient adaptation plans by analyzing different social vulnerabilities present in towns and cities. The general aims of the present study are i) to provide a replicable and scalable spatially explicit open-access methodology, performed in a GIS environment at urban and suburban scales, to assess the heat-related risk from HWs by taking into account the unequal distribution of social vulnerabilities of sensitive social groups; and ii) to propose the first climate justice heat-related risk index for the design of inclusive and just adaptation plans. The specific aims are to i) identify the period of HWs and map critical UHI hotspots at suburban scale; ii) map the heat-related risk to vulnerable social groups (elderly aged $>$ 65 years, elderly living alone, children aged $<$ 5 years, households with an income $<$ 10,000 €/year, and foreign residents); and iii) propose a global climate justice risk index for all the vulnerable categories considered.

2. Data and methodology

2.1. Study area: A geographical framework of the city of Padua

This study is focused on the urban territory of Padua, a medium-sized city located in the Po floodplain within the Veneto Region (NE Italy) approximately 20 km from the Venice lagoon (Fig. 1). The municipal territory spans 92.8 km^2 and has a resident population of 208,702 (Comune di Padova, 2022). The city was built within the Brenta and Bacchiglione rivers; ancient Venetian walls and canals surround the historic urban core. From the end of the 19th century Padua expanded beyond its historical limits due to demographic growth and economic and industrial development. As in other European cities, the urban development was shaped by medium-density residential districts around the city center and sparse new buildings or complexes on the urban fringes between the core city and the surrounding countryside. The

Table 1
List of all spatial and weather data (including metadata) used to perform GIS modelling.

Meteorological data	Source	Period	Frequency of sampling	Variables
	ARPAV (Regional Environmental Protection Agency)	6 February 1992 to 2 October 2022	Hourly	2 m air temperature
Satellite images	**Source**	**Landsat 9 Sensing Date and Hour (UTC)**	**Landsat Identifier**	**Image Quality**
	USGS Earthexplorer	03/07/2022 09:58	LC09_L1TP_192028_20220703_20220703_02_T1	9 out of 9
		04/08/2022 09:58	LC09_L1TP_192028_20220804_20220804_02_T1	9 out of 9
Administrative boundaries	**Source**	**Layer description**		
	Veneto Region Geoportal	Vetctor layer of Padua's administrative boundaries		
	Municipality of Padua's webgis	Raster layer of Padua's Urban Units		
	Edimap	Vector layer of CAP areas		
Land Use and Land Cover Data	**Source**	**Layer description**		
	Copernicus - Corine Land Cover	Vector layer of land use classification		
	ISPRA - National Environmental Protection Agency	Raster layer of impervious surfaces		
Socio-demographic data	**Source**	**Layer description**	**Variables**	
	Statistical report 2022 - Statistical bureau of Padua's Municipality	Population statistics in each Urban Unit	Total population, population density, % of foreigners; % of children under 5, % of elderly over 65, % of elderly over 65 living alone	

Table 2
Identification of heatwaves, maximum air temperatures, and above-threshold air temperatures in summer 2022 (Ground weather station in Legnaro).

Heatwave period	Duration (Days)	Max air temperature for each day Legnaro Ground Weather Station (°C)	Temperature above HW threshold (°C)
02/07/2022 – 05/07/2022	4	32.4; 34.3; 35.1; 32.8	0.4; 2.3; 3.1; 0.8
21/07/2022 – 23/07/2022	3	34.4; 36.1; 35.1	0.4; 2.1; 1.1
04/08/2022 – 06/08/2022	3	34.8; 35.8; 35.4	0.1; 1.2; 1.4

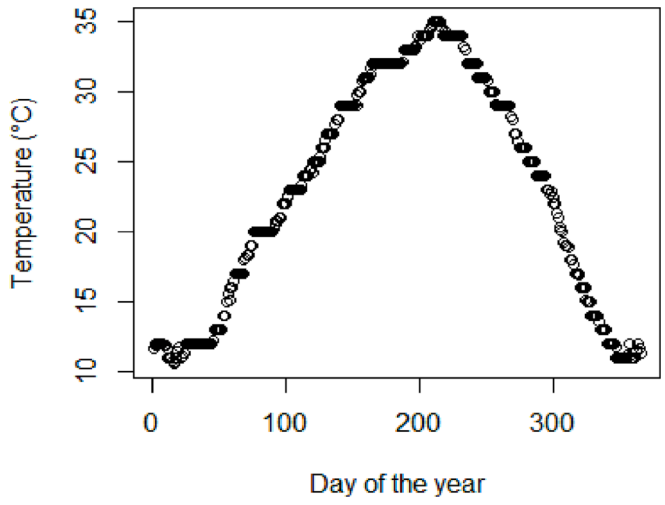

Fig. 2. 90° percentile threshold (°C) for HW identification for each day of the year.

urbanization processes led to a territorial fragmentation of *peri*-urban natural and rural areas. The urban fabric is, therefore, at present highly heterogeneous and fragmented, with a mix of new residential areas and green spaces as well as commercial and industrial districts (Fig. 1).

Due to urban expansion and infrastructuring, this territory is one of the most affected in Italy by soil sealing. In fact, the latest annual report on soil sealing and ecosystem services, published by the National Institute for Environmental Protection (Munafò, 2022), ranked Padua as the fifth largest city in Italy, with >100,000 inhabitants, with sealed surfaces and high yearly rates of soil sealing. Recent studies which adopted GIS modelling techniques on high-resolution multispectral images to map soil sealing estimated that about 50% of the urban surface is currently sealed (Peroni et al., 2019; Pristeri et al. (2020); Pristeri et al. (2021). As is widely documented, when HWs affect an urban territory extremely affected by soil sealing, the impacts of UHIs on the area are magnified (Phelan et al., 2015; Du et al., 2016; Kotharkar & Surawar, 2016; Yue et al., 2019; Peroni et al., 2022). Moreover, urban green areas are spatially scattered within the municipality with the lowest values per capita in the historic core and the northern sectors (1–10 m^2/inhabitant) (Pristeri et al., 2021).

Lastly, the urban territory of Padua is reported to be affected by HWs and UHIs combined during the summer (Busato et al., 2014; Noro et al., 2015). Recent estimates by Todeschi et al. (2022) indicated that land surface anomalies within the metropolitan area of the city might reach 6.8 °C. Therefore, Padua, in terms of size, population, urban fabric, and the UHI phenomenon, has various characteristics in common with other cities in Europe.

2.2. Input data

All input data and software used in this research are completely open access and open source. Statistical and spatial analysis were performed by using RStudio (v.2022.07.2) and QGIS (v.3.22.13). All geographic data were re-projected into the spatial reference system WGS 84/UTM zone 32N (EPSG 32632). All data used in this study are summarized in Table 1.

2.2.1. Meteorological data

Meteorological data used in this research are provided by the Regional Environmental Agency (ARPAV, https://www.ambienteveneto.it/datiorari/datiSensOrari.php?cd=222&an=2022). For HWs identification we used hourly 2 m air temperature data from the official weather station located in Legnaro (Province of Padua, geographical coordinates: 11.95217201 W; 45.34734845 N), which is 8 linear km from the city centre of Padua, within a rural context. The meteorological series starts 6 February 1992 and ends 2 October 2022. We did not consider the official weather station located within the

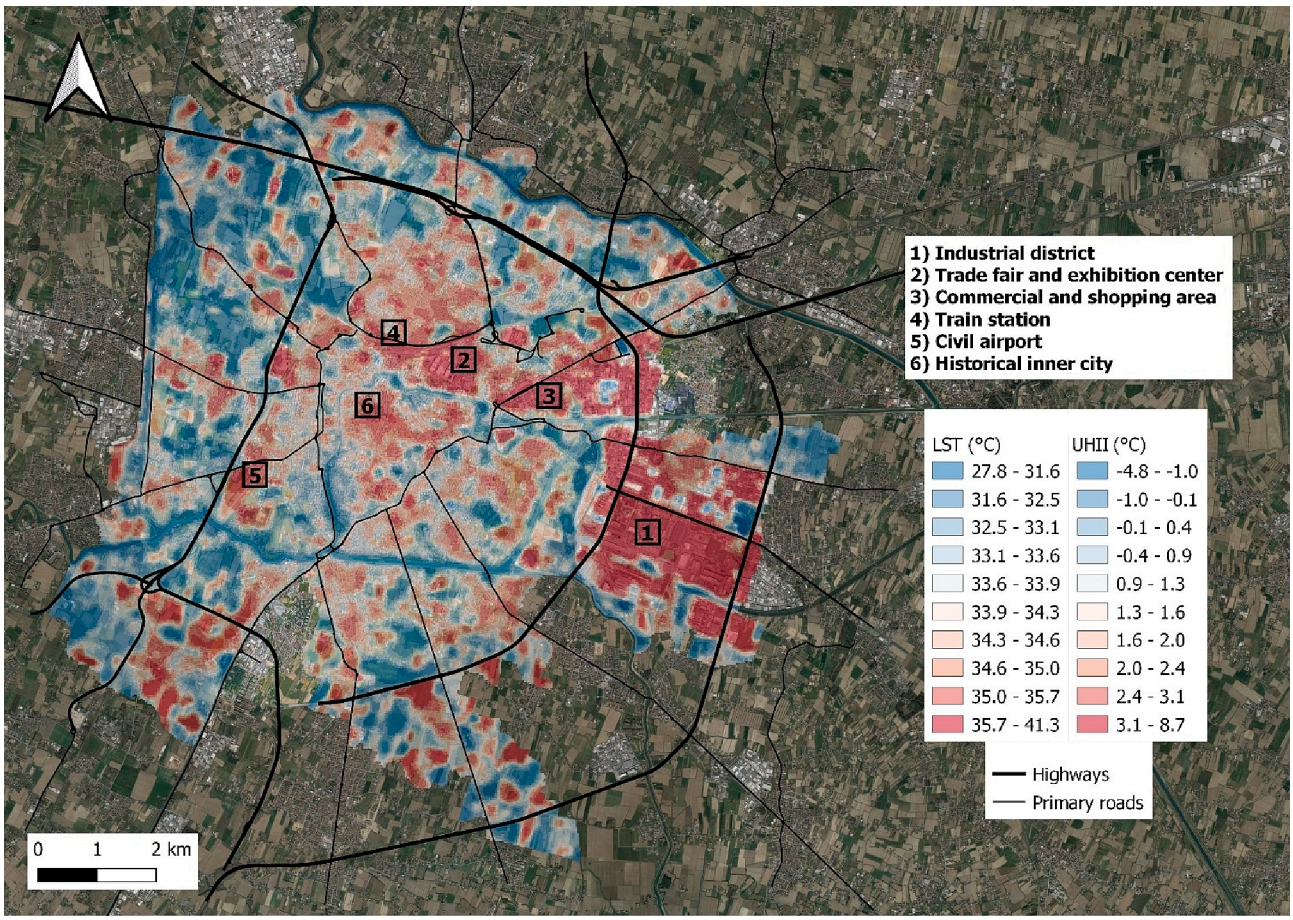

Fig. 3. LST and UHI intensity in the municipality of Padua. UHI hotspots – defined as 90° percentile of LST distribution – are numbered in the boxes: 1) industrial district, 2) trade fair and exhibition center, 3) commercial and shopping area, 4) train station area, 5) civil airport, and 6) historic inner city.

municipality as ARPAV changed the position in 2020 and no homogeneous time series are available in the municipality according to the meteorology and climatology unit of ARPAV.

2.2.2. Satellite data

Landsat 8 and 9 satellite data from the United States Geological Survey (USGS, https://earthexplorer.usgs.gov/) are the baseline dataset for the spatial calculation of Land Surface Temperature (LST). Landsat 8 satellites have acquired images since 2013 with a frequency of 16 days. From 2021, by combining acquired images from Landsat 9, a two-fold increase in frequency was pursued, with an overall revisiting time of 8 days, always at the same time of the day (Landsat 8 and 9 together). In this study we used band 4 (Red), band 5 (NIR) and band 10 (TIR-1) for spatial analyses. Bands 4 and 5 present a geometric resolution of 30 m, while TIR-1 presents 100 m pixel size. We therefore clipped satellite scenes within the spatial domain adopted in this research, defined as a buffer zone of 15 km radius from the centroid of the Padua municipality. All Landsat images acquired within the HW periods in summer 2022, as defined in section 2.2, were selected. Exact time of image acquisition, USGS Landsat identifier and image quality are shown in Table 1.

To better understand the UHI phenomenon we searched for all available Landsat 8 and 9 scenes in the JJA period (2022), according to HWs meteoclimatic analysis. Hence, due to factors such as urban morphology, meteorological conditions (e.g. wind speed and direction, relative humidity, atmospheric pressure) and LULC, which makes UHI a complex phenomenon characterised by high spatial and temporal variability, we averaged LST values of available satellite scenes (Liao et al., 2021; Peng et al., 2022; Mentaschi et al., 2022).

2.2.3. Administrative boundaries and urban units

The spatial domain of the socio-demographic analysis is represented by the official boundaries of the municipality of Padua (93 km^2), represented by a vector layer retrieved from the geoportal of Veneto Region (websource: https://idt2.regione.veneto.it). The municipal territory of Padua is divided into 40 Urban Units (UUs), which are the smallest area in which the statistics office collects and aggregates socio-demographic data (see Appendix B). UUs cartographic layer was manually georeferenced and digitized from a pdf map downloaded from the official webpage (https://www.padovanet.it/sites/default/files/attachment/02%20Territorio.pdf). To perform geographic analyses on economic indicators (low-income residents) we also used the Postal Code (CAP, the italian equivalent of ZIP code) as spatial units.

2.2.4. Land use and land cover data

Two typologies of Land Use and Land Cover (LULC) were used in this study. The first LULC dataset is represented by the latest Corine Land Cover (CLC) 2018 vector layer, acquired from the Copernicus Programme database (European Commission, 2022, websource: https://land.copernicus.eu/pan-european/corine-land-cover/clc2018). CLC data is currently the most reliable land cover database for Europe, since it classifies land cover into 44 different classes and is updated every 6 years. In this study we used CLC first level of classification of LULC to identify the vegetated areas within 15 km radius from the centroid of the municipality.

The second LULC layer is represented by the impervious surfaces at 10 m geometric resolution, annually updated in the "National report on soil sealing and Ecosystem Services", provided by the Italian Institute for Environmental Protection and Research (Munafò, 2022). By using this raster data with binary values on sealing we performed the correlation

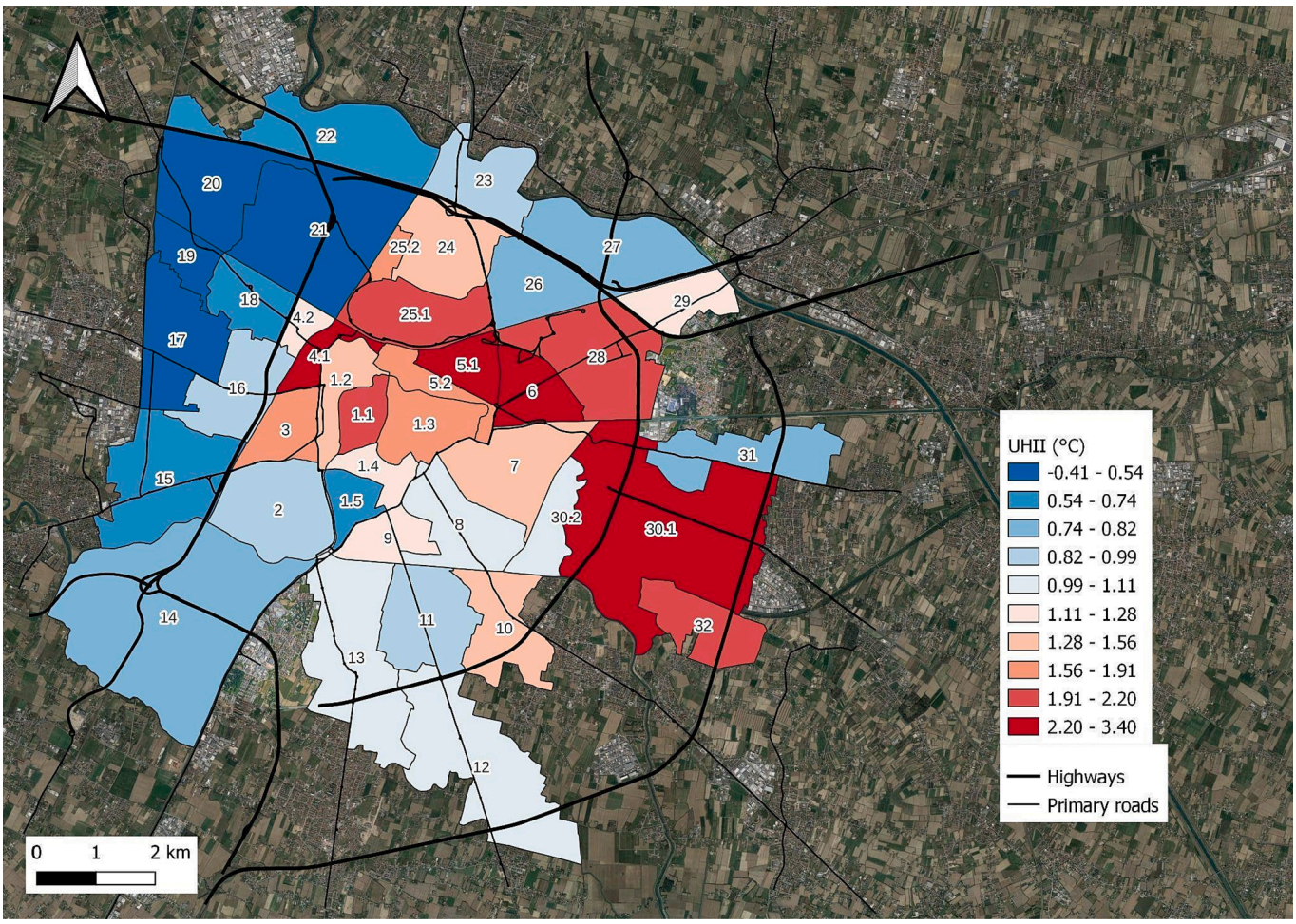

Fig. 4. Mean UHII (°C) for each numbered UU.

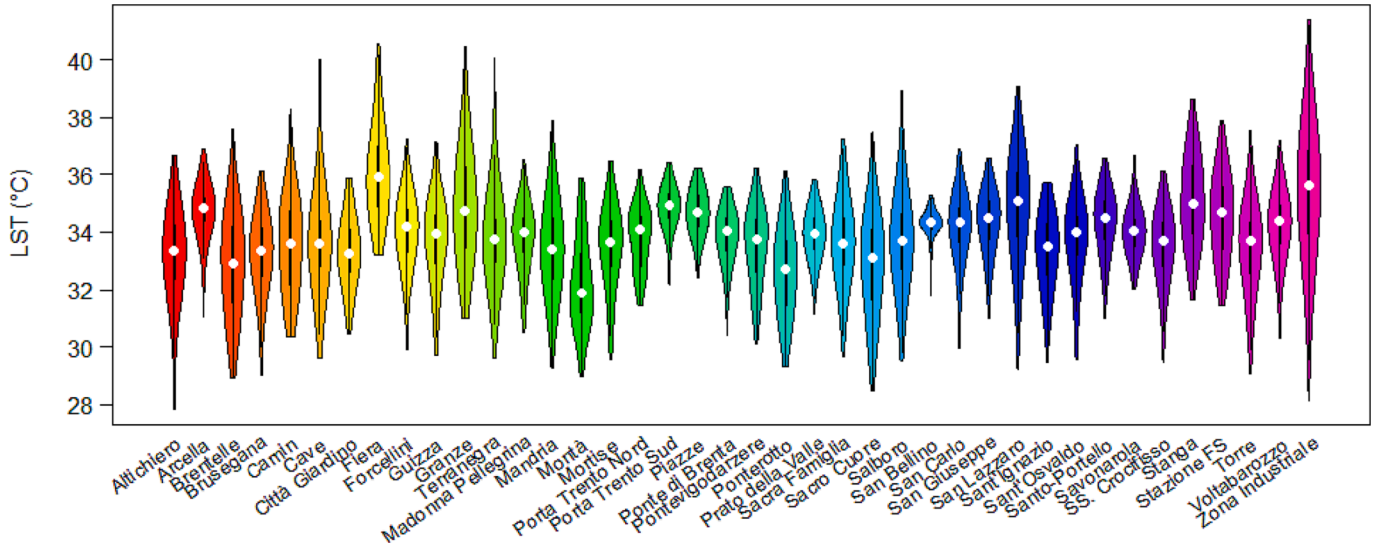

Fig. 5. Violin plot of LST distribution in Padua's Urban Units.

analysis among impervious surfaces and LST values.

2.2.5. Socio-demographic data

Socio-demographic data were acquired from the statistical report published by the statistics office of the municipality of Padua ("Annuario Statistico" 2022, https://www.padovanet.it/informazione/padova-cifre). From this report we calculated at UU level the following parameters (see attachment 1): i) total population, ii) population density, iii) percentage of children under 5 years, iv) percentage of elderly over 65 years, v) percentage of elderly over 65 living alone, and vi) percentage of foreign residents. Household income data are downloaded from the Italian Ministry of Economy and Finance website (https://www1.finanze.

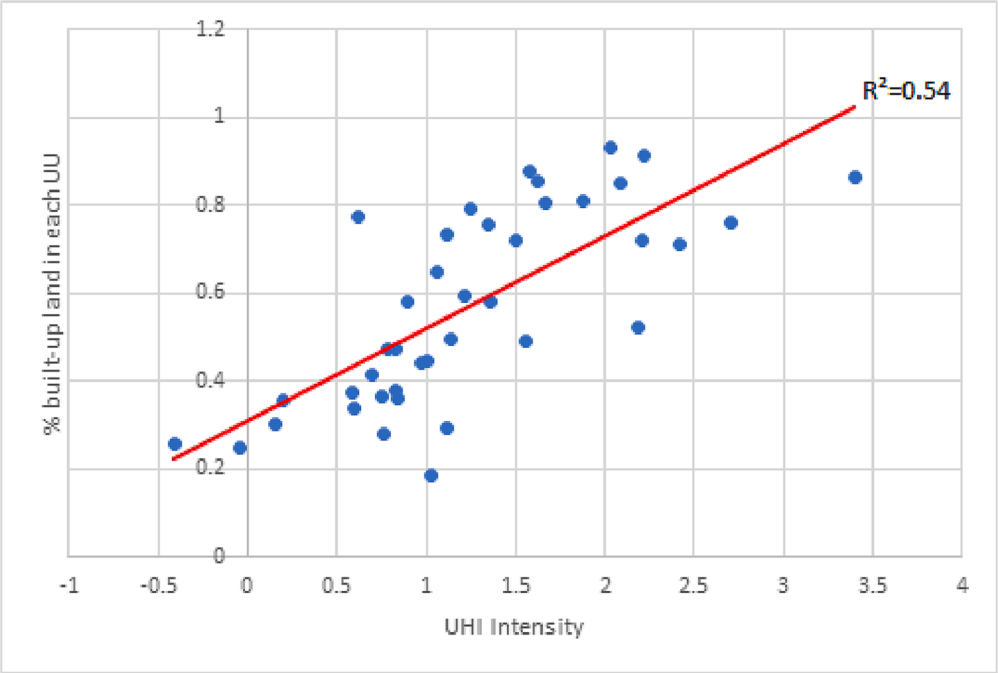

Fig. 6. Scatterplot of UHI intensity and percentage of impervious surfaces in Padua's Urban Units. The red line indicates the OLS regression. (For interpretation of the references to color in this figure legend, the reader is referred to the web version of this article.)

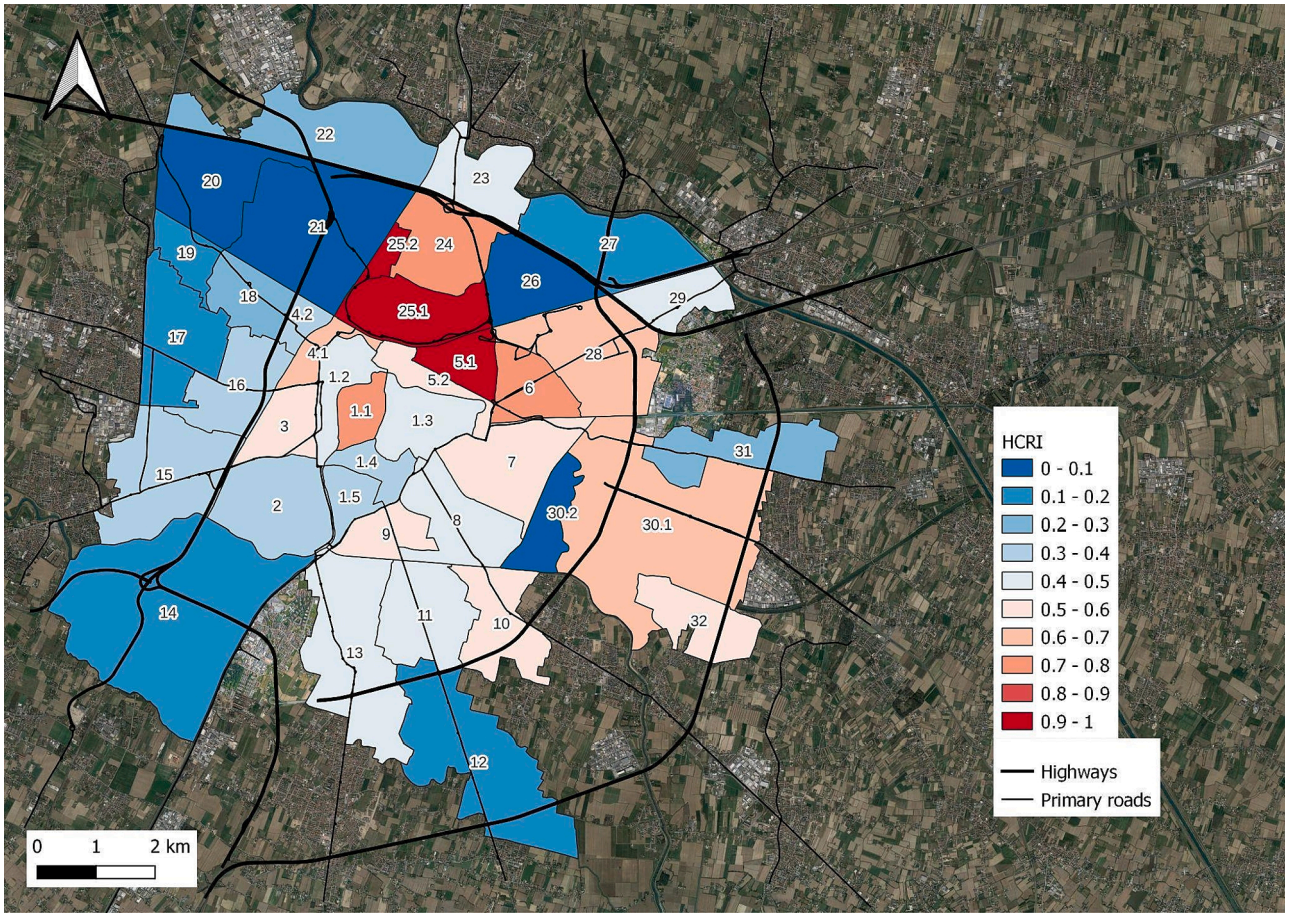

Fig. 7. HCRI in Padua's Urban Units.

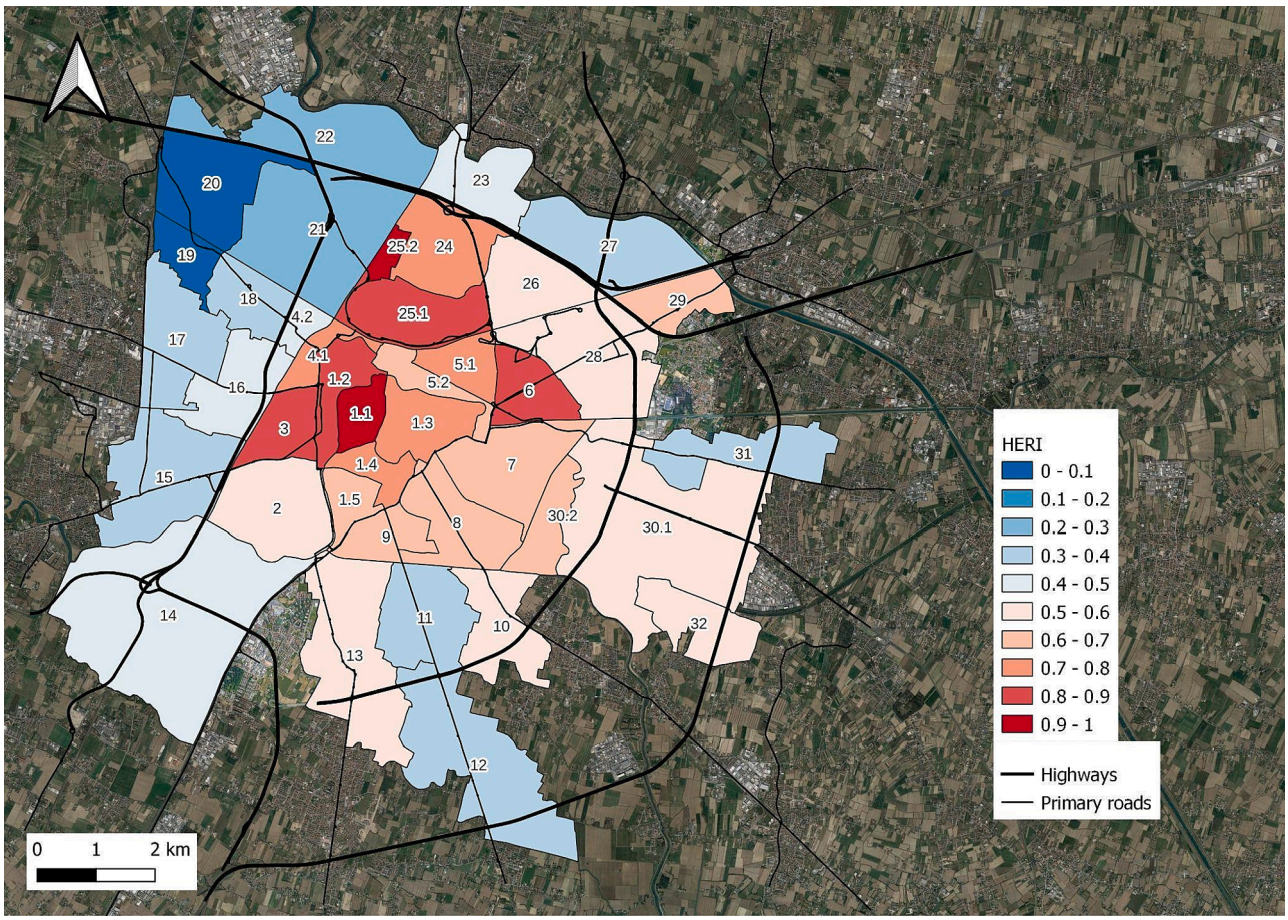

Fig. 8. HERI in Padua's UUs.

gov.it/finanze/analisi_stat/public/index.php?opendata = yes). Such demographic and social categories represent the most vulnerable categories to extreme heat events (Vanos 2015; Nayak et al., 2018). It is well documented in the literature that elderly people are one of the social categories most vulnerable to heat stress (Vandentorren et al., 2006; Conti et al., 2007; Åström et al., 2011); a sub-group is represented by elderly people living alone, because in case of an emergency related to heat stress there is no one else in the house that can provide first aid or call an ambulance. Children under 5 years are vulnerable to HWs because heat stress causes an increase of morbidity in the renal system and respiratory diseases (Xu et al., 2014; Arsad et al., 2022). Low-income households have less possibility to implement adaptation solutions to face extreme heat in the house, like air conditioning or thermal insulation (Sakka et al., 2012; Churchill & Smyth, 2021). Finally, foreigners are less responsive to public health communication campaigns commonly used to inform the population about good practices to implement during heat waves, due to linguistic barriers (Matthies & Menne, 2009; Messeri et al., 2019).

2.3. Heat wave periods identification

There are different methodologies in the literature to identify HWs. We used the statistical definition provided by Russo et al. (2015); it is currently the most adopted methodology, and it is also used by the Regional Environmental Protection Agency (ARPAV, 2022). The present methodology identifies a period of HW if the daily maximum air temperature of the day "d" exceeds the "A_d" threshold for at least 3 consecutive days, as defined by the following Equation (1):

$$A_d = \bigcup_{y=1992}^{2022} \bigcup_{i=d-15}^{d+15} T_{y,i} \quad (1)$$

where:

A_d = threshold, expressed in °C, that must be exceeded by the maximum temperature of a specific day d to become a potential day of a HW period.

y = year of the weather data time series.

T = 90th percentile.

In this study for HWs identification and UHI spatial analyses we focused on the Summer (2022) period, commonly defined as June, July and August (JJA).

2.4. Land surface temperature analysis

LST within a 15 km buffer radius from the centroid of the municipality of Padova was calculated from Landsat thermal band (TIRS1). The methodology follows USGS LST guidelines (Zanter, 2018). The calculation of UHII – the difference between background rural and highest urban temperatures (Oke, 1973) – follows the methodology by RUS-Copernicus (Serco Italia SPA, 2018). All LST calculations were performed pixel-by-pixel for each Landsat scene, by using R Studio, a free and open-source statistical software.

For a complete description of the emissivity and LST calculation by using NDVI see Annex A.

2.5. Urban heat island intensity and relationship with land cover

Urban Heat Island Intensity (UHII) is defined as the difference between background rural and highest urban temperatures (Oke, 1973).

UHII calculation is based on the following Equation (2):

$$UHII = \Delta T_{u-r} = T_u - T_r \quad (2)$$

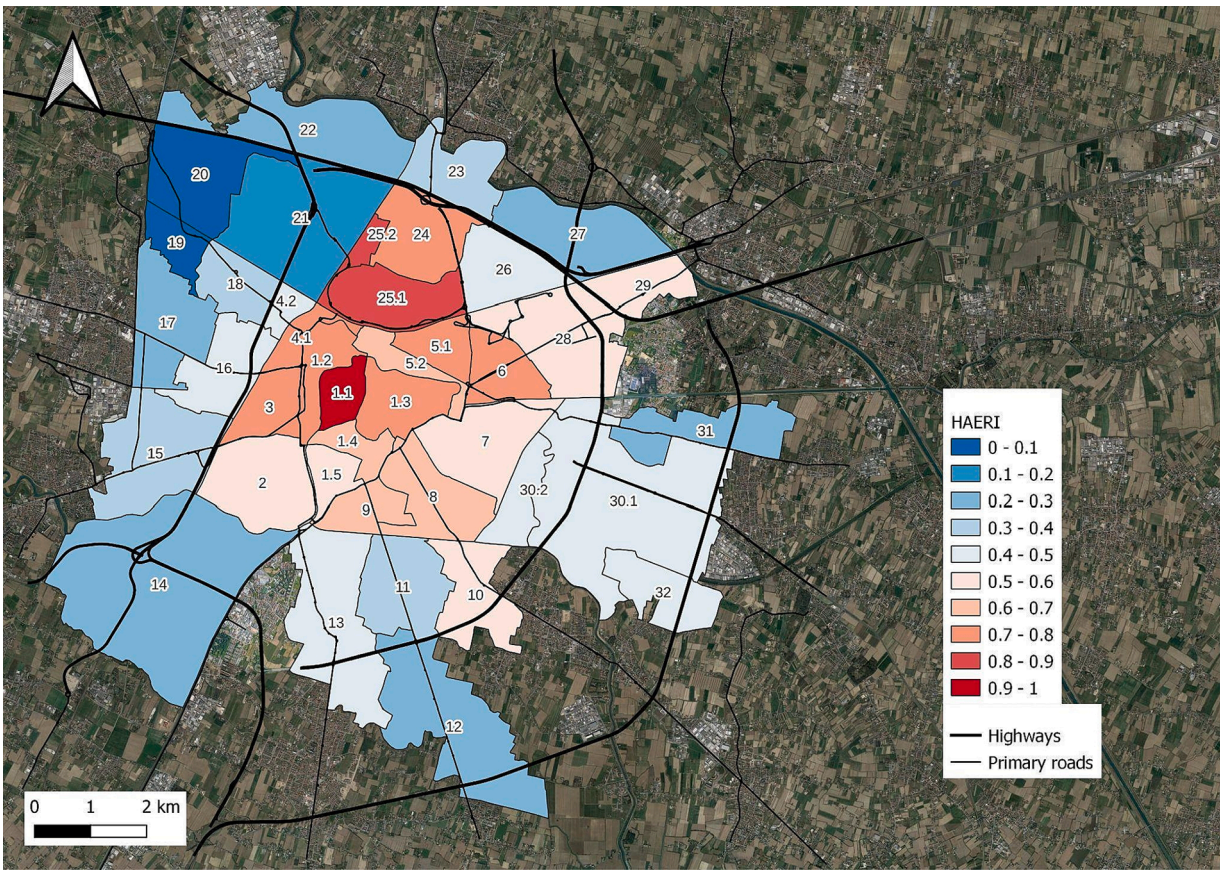

Fig. 9. HAERI in Padua's UUs.

where:

T_u = urban temperature.

T_r = rural temperature.

The adopted methodology to assess UHII is based on Serco Italia SPA (2018) and it consists in subtracting from each pixel in the study area the mean LST value of a set of sampling points which are representative of non-urban areas (Pins). Each pin of the set has the following characteristics:

1) It is the centroid of the union of contiguous CLC polygons with level 1 classes "agricultural areas" or "forest and semi-natural areas";
2) It is located inside an annulus centred in the centroid of the municipality of Padua, with radiuses of 10 km and 15 km respectively.
3) It is at least 350 m from CLC class "Anthropic impervious surfaces".

As LULC represents an important contribution in UHI (Sangiorgio et al., 2020), we also investigated the relationships between UHII and the presence of impervious surfaces derived from ISPRA raster file (2022), by performing a pixel-by-pixel Ordinary Least Square (OLS) Regression. By this methodology we aim to test if there is a negative correlation between LST and impervious surfaces, as found by Todeschi et al. (2022). We performed the same OLS regression also between mean UHII and percentage of impervious surfaces in sub-administrative areas (UUs and CAPs).

2.6. Heat-related risk assessment indexes

In this subsection we present five indexes for assessing climate inequalities among different UUs within the municipality of Padua: Heat-related Child Risk Index (HCRI), Heat-related Elderly Risk Index (HERI), Heat-related Alone Elderly Risk Index (HAERI), Heat-related Foreigners Risk Index (HFRI) and Heat-related Low-Income Risk Index (HLIRI). These indexes aim to rank sub-administrative areas in terms of heat-related risk for five different vulnerable social groups as described in section 2.1.5: i) children under 5, ii) elderly over 65, iii) elderly over 65 living alone, iv) foreigners and v) low-income households (<10.000 €/year).

The general construction of these five climate-risk indexes, each one based on a single vulnerable group, is represented in Eq. (3). All the risk indexes here presented are the weighted sum of the three components of risk: Vulnerability, Exposure and Hazard (Tomlinson et al., 2011). All three components of risk are normalized from 0 to 1 by applying a min–max normalization method on sub-administrative areas records.

$$R_{i,j} = 0.25V_{i,j} + 0.25E_j + 0.5H_i \quad (3)$$

where:

$R_{i,j}$ = heat-related risk index for vulnerable category i in the sub-administrative area j.

$V_{i,j}$ = normalised spatial density of vulnerable category i in the sub-administrative area j.

E_j = normalised exposure, expressed as the population density in the sub-administrative area j.

H_i = normalised hazard, expressed as the average UHII in the sub-administrative area j.

2.7. UHI Heat-Related risk Index

The Urban Heat-Related Risk Index (UHRI) is based on the same structure of the indexes presented in section 2.7 but simultaneously considers multiple vulnerable groups together: children, elderly and foreigners. UHRI for each UU is built as described in Eq. (4).

$$UHRI_j = 0.125\sum V_{k,j} + 0.125E_j + 0.5H_j \quad (4)$$

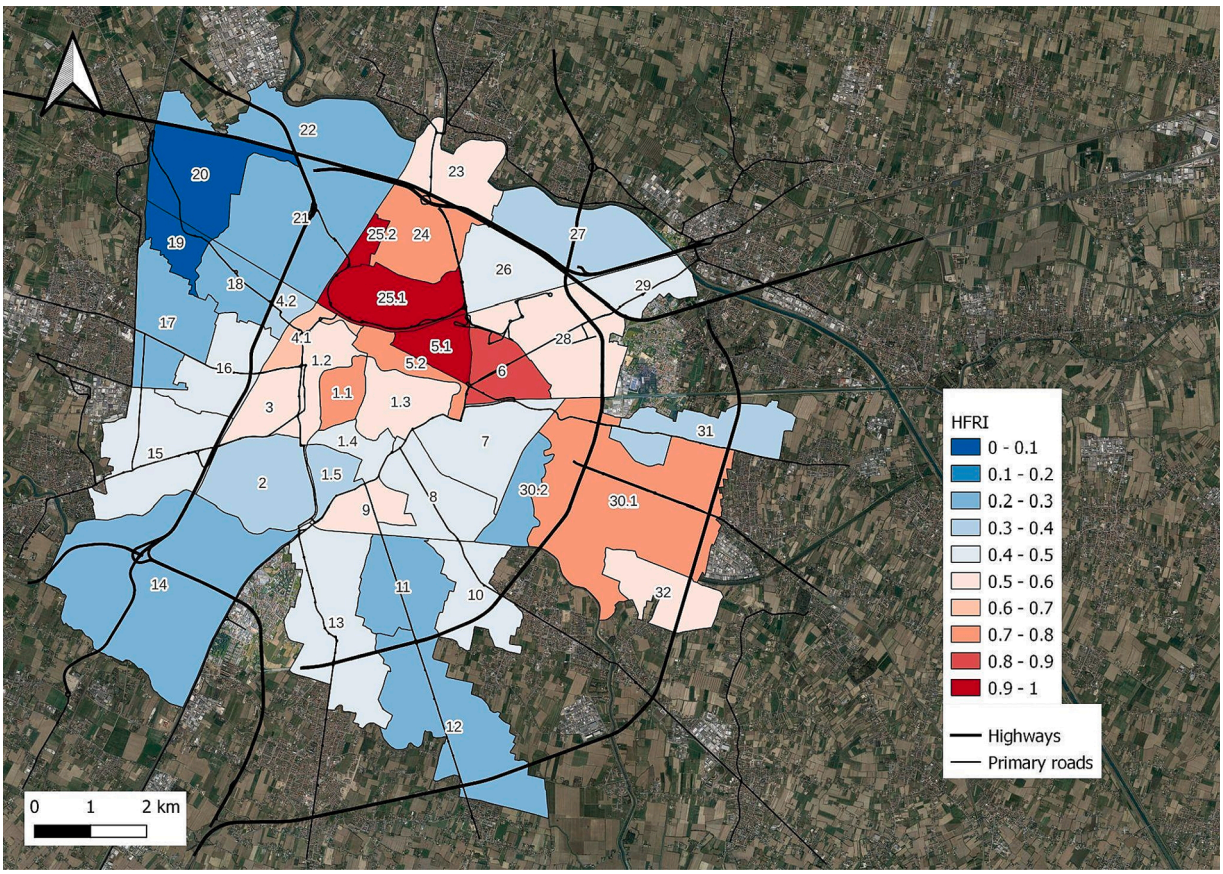

Fig. 10. HFRI in Padua's UUs.

where:

$GHRI_j$ = Global Heat-Related Risk Index for UU j.

$V_{k,j}$ = normalized spatial density in UU j of vulnerable group k.

E_j = normalized Exposure, expressed as the population density in the sub-administrative area j.

H_j = normalized Hazard, expressed as the average UHII in the sub-administrative area j.

3. Results and discussion

This section is structured into three subsections. The first subsection presents the results of an LST analysis in the city of Padua during HWs which aimed to identify UHI hotspots as defined in section 2.5. The second subsection highlights the spatial distribution of those social categories which are most vulnerable to heat stress as well as the related UHI risk indexes. In the last subsection the Global UHI Risk Index is presented to identify urban areas where there is an urgent need to implement just and socially equitable adaptation measures to reduce climate risk.

3.1. Mapping and identifying UHI hotspots at suburban scale in summer 2022

A meteo-climatic analysis undertaken to identify HW thresholds detected three HW periods in Padua during summer 2022: the first at the start (2–7) of June with a maximum T of 35.1 °C, the second in July (21–23) with a maximum T of 36.1 °C, and the third in August (4–6) with a maximum T of 35.8 °C. Details of the duration and temperature values above the HW thresholds are shown in Table 2. It is important to note that HW periods were based on a 30-year time series of air temperature data measured at the ARPAV weather station in Legnaro. The HW threshold for each day of the year, as described in section 2.2, is represented in Fig. 2.

A detailed search of satellite images within the identified HW timeframes found two Landsat 9 scenes with no cloud cover over the study area. These scenes were used for LST calculations and UHI identification in summer 2022, the first from 3 July and the second from 4 August (Table 1). Fig. 3 shows the map of LST and UHII in the municipality of Padua. The latter is expressed as the difference between the LST value of every single pixel and the rural pins' mean LST value, as described in section 2.5.

Spatial thermal analysis performed at urban and suburban scale highlights that the highest values of LST seems to be localized mainly on strongly sealed areas of the city, especially in the eastern (industrial district) and northern sectors, with surface temperatures ranging from 36 to 41 °C. Other areas with high LST values are scattered within the urban territory, which has a complex urban fabric, according to specific local conditions such as the presence of green areas (e.g., parks and agricultural lands) or water channels and the degree of imperviousness. We therefore tested this hypothesis by performing a pixel-by-pixel Ordinary Least Squares (OLS) regression analysis as described in section 2.5. The regression coefficient β indicates that over impermeable surfaces the LST is, on average, 1.42 °C higher than in permeable areas. The regression is significant ($\alpha < 0.001$).

Calculation of the UHII based on the 25 pins previously identified shows an average LST within the municipality of 33.8 °C ($\sigma = 1.7$, min = 27.9, max = 41.4). As expected, the highest UHII values are mapped especially in correspondence of wide continuous impervious surfaces, with temperature anomalies ranging from 3 to 8 °C, while lower values are found over permeable surfaces.

Spatial analysis of UHII areas in which only the upper decile was selected highlights that values of surface temperature anomalies range from 3.1 °C to 8.7 °C. We therefore identified six different UHI hotspots within the study area: 1) the industrial district (namely, ZIP), 2) the

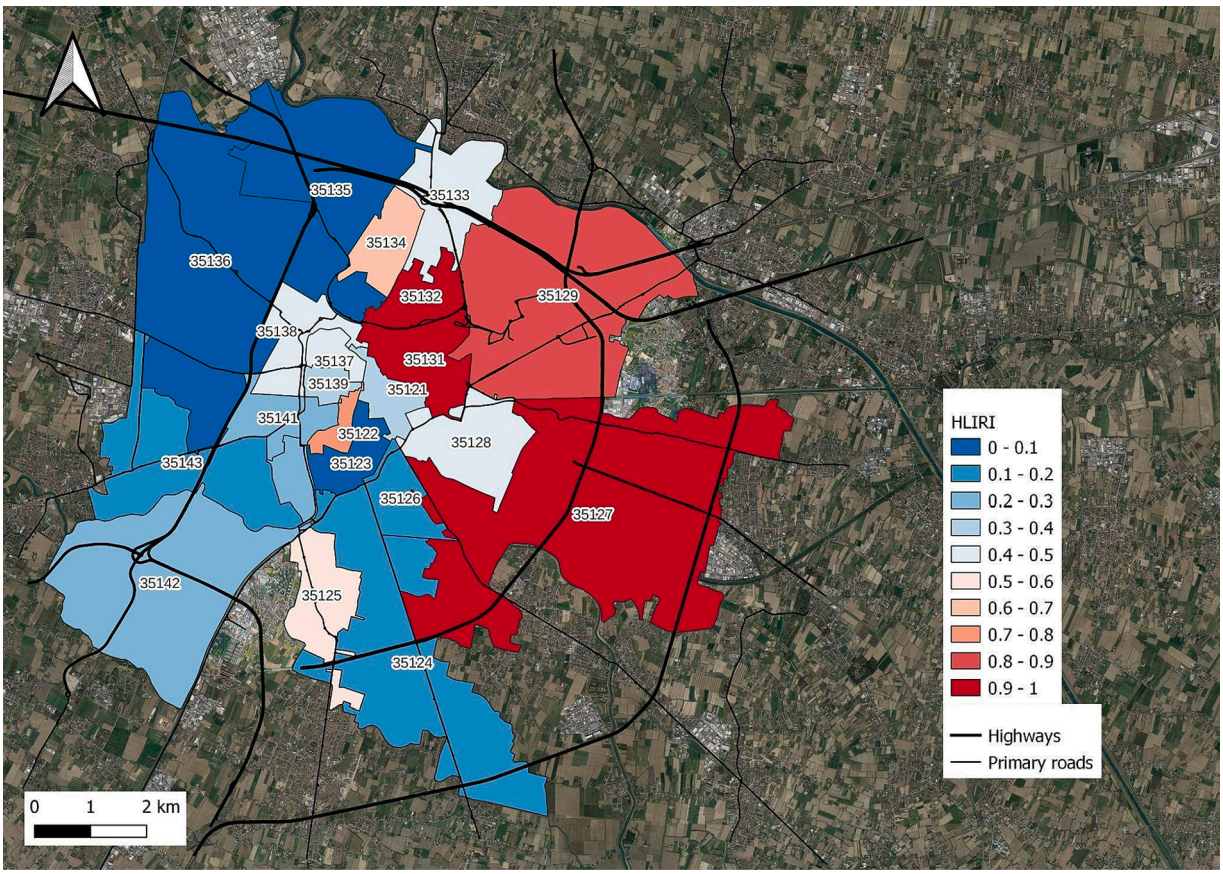

Fig. 11. HLIRI in Padua's CAPs.

trade fair and Exhibition Center, 3) the commercial and shopping area, 4) the train station area, 5) the civil airport, and 6) the historic inner city. In general, it is possible to geovisualize from the map that the city center and high-density *peri*-urban residential areas are most affected by the UHI effect (Fig. 3).

3.1.1. Distribution of urban heat island intensity at suburban scale: Urban units' thermal analysis

To better investigate UHI effects on specific urban sectors as well as to provide useful spatial information for future inclusive climate-resilient adaptation planning, we performed a UHII analysis at suburban scale, specifically on the administrative urban unit (UU) level (Fig. 4). Spatial analysis highlights that the UUs most impacted by UHII are those in the central, northern, and eastern sectors of the municipality; more specifically, the warmest UUs are 5.1 – exhibition center, 30.1 – industrial district, and 6 – commercial area, which have UHIIs of 3.4 °C, 2.7 °C, and 2.4 °C on average, respectively. The cooler UUs are mainly located in the fringe running from the southwest to the northwest sectors of the municipality, specifically 19 – Montà, 20 – Ponterotto, and 21 – Sacro Cuore, which have UHIIs of −0.4 °C, 0 °C, and 0.2 °C, respectively.

It is worth noting that the urban fabric and land use of the UUs of Padua are very heterogeneous (Pristeri et al., 2020). Apart from the UUs of the historic center, which are more homogeneous and where there is a high prevalence of old, residential, and commercial buildings, most neighborhoods are very heterogeneous and include different types of isolated residential areas, green spaces, canals, and agricultural parcels. The internal UHII variability for each UU is visually represented in the violin plot in Fig. 5. The area of each "violin" in the plot is proportional to that of the related UU listed in the X axis. The horizontal width of each "violin" is proportional to the area of the UU with an LST in the Y axis. As expected, central UUs have less internal variability in terms of LST than outlying UUs.

Finally, to describe the spatial relationships among thermal anomalies and soil sealing within UUs we performed an OLS regression model between the percentage of impervious surfaces and the mean UHII. The OLS analysis shows a positive correlation between the two variables with the regression coefficient β, which indicates an average increase of 0.3 °C on every 10% of soil sealing (Fig. 6). The R^2 value of the OLS regression is 0.54.

3.2. Mapping heat-related risk for vulnerable social categories for inclusive climate-resilient planning

In this subsection we present the results of the heat risk assessment for vulnerable social categories in Padua. The methodology shown in section 2.7 identifies five different vulnerable categories: the elderly, the elderly living alone, children, foreigners, and low-income residents. For each vulnerable social category, we calculated the risk index for the UHII from 0 (lowest risk) to 1 (highest risk).

3.2.1. Heat-related child risk index

The Heat-related Child Risk Index (HCRI) ranks the UUs on different levels of risk to children aged less than five. We found that the HCRI is higher in the following UUs: 5.1 – Fiera, 25.1 – Arcella, and 25.2 – San Bellino. In fact, population density in these UUs is high, with a large number of children under five and high UHII. In general, lower HCRI values are distributed in the UUs on the periphery of the municipality where – even though there is a high percentage of children – UHII and population density are lower (Fig. 7).

3.2.2. Heat-related elderly risk index

Similarly, to the HCRI, the Heat-related Elderly Risk Index (HERI) analysis classifies UUs in terms of risk for those aged > 65 years. Spatial analysis of the risk to elderly people highlights that the most critical UUs

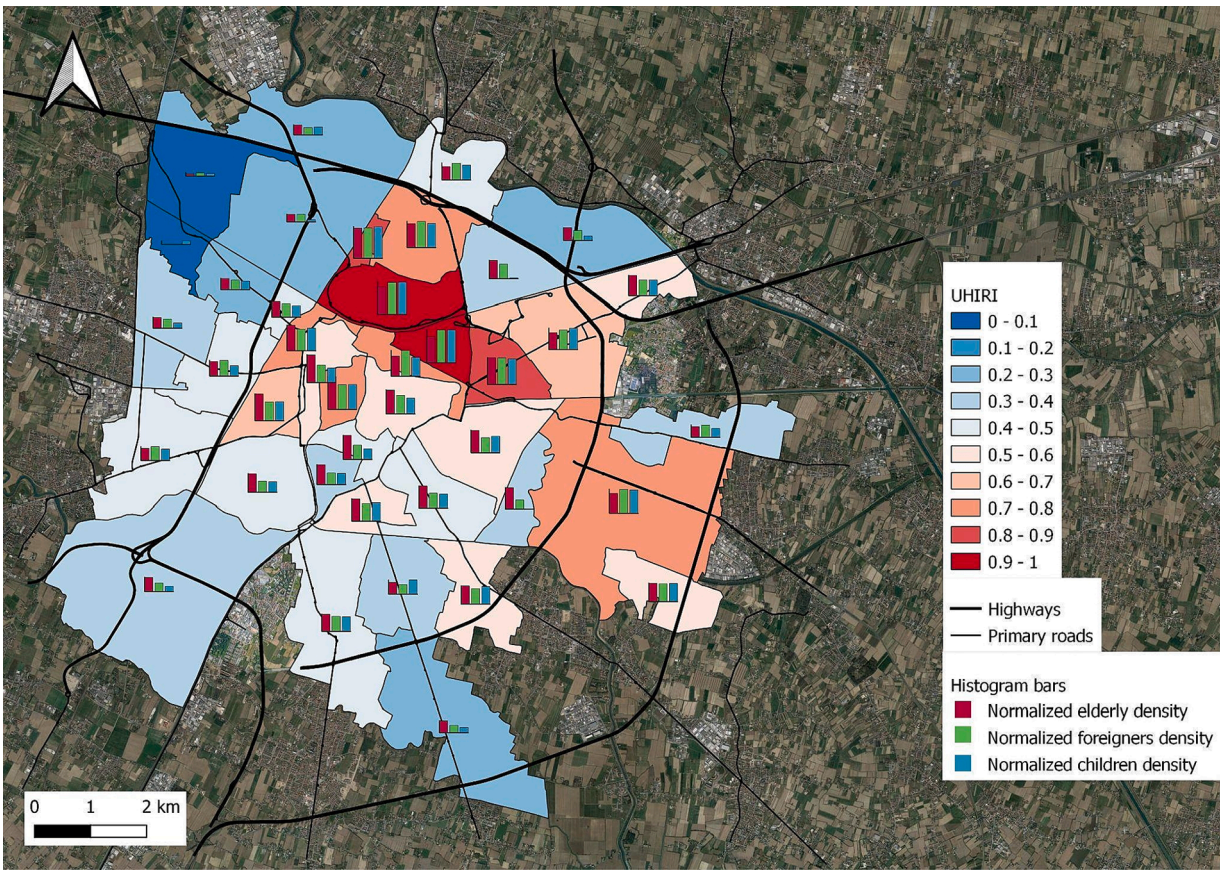

Fig. 12. UHIRI in Padua's UUs. Histogram bars represent normalized density of elderly (red), normalized density of foreigners (green), and normalized density of children (blue). (For interpretation of the references to color in this figure legend, the reader is referred to the web version of this article.)

are 1 – Piazze, 25.2 – San Bellino, and 2 – Savonarola (Fig. 8). As expected, the central UUs are most at risk of heat stress, with peaks in residential areas where there are more elderly residents, such as 2 – Savonarola, 3 – San Giuseppe, and 1.4 – Prato della Valle.

3.2.3. *Heat-related alone elderly risk index*

The spatial pattern for the Heat-related Alone Elderly Risk Index (HAERI) in the various UUs of Padua does not substantially differ from the HERI analysis: The historic city center and nearby UUs are most impacted by UHII (Fig. 9). It is important to stress that HAERI is probably the most crucial index as the heat-related risk to elderly people who live alone is particularly critical as, in the event of a health emergency, no support is available directly from their residence.

3.2.4. *Heat-related Foreigners' risk index*

The Heat-related Foreigners' Risk Index (HFRI) spatial analysis allows us to classify the UUs in terms of heat-related risk to foreign residents. The highest HRSI values are in the six UUs located in and around the central train station, especially 25.1 – Arcella, 25.2 – San Carlo, and 5.2 – Fiera (Fig. 10). In fact, a high percentage of foreign residents live in these UUs, and there is high population density and high UHII. Due to different factors related to migration policies, housing prices, and cultural aspects, most foreign residents are located in these UUs.

3.2.5. *Heat-related low-income risk index*

Spatial analysis highlights that the heat-related risk for low-income residents (<10,000 €/year) is higher in the northeastern sector of the municipality, where the combination of the UHII related to the high prevalence of industrial and commercial areas as well as the central station result in higher values (Fig. 11). In fact, according to the spatial distribution of low-income residents and the UHII these sectors are the most impacted (Appendix B). One anomaly is represented in the CAP 35122, which houses the highest percentage of low-income residents (36%) but generates the highest income from house rentals.

It is important to highlight that the Heat-related Risk for Low-income Residents Index (HLIRI) was spatially developed using the same structure as the other heat-related risk indexes for the vulnerable categories presented above; unfortunately, however, since no data about income were available at UU level it is based on different spatial units which refer to the postal code boundaries (see section 2.1.3).

3.3. *Urban heat-related risk index*

The Urban Heat-related Risk Index (UHIRI) indicates the level of heat-related risk for three vulnerable categories: the elderly, children, and foreigners. Spatial analysis of the UHIRI showed that the highest values of UHIRI are located in UU 5.1 – Fiera, in which the main contribution to the UHIRI is the UHII, since average values are much higher than in the other UUs (3.4 °C). The second-ranked UU for UHIRI is 25.1 – Arcella, in which all variables related to total population, population density, and percentage of foreigners are very high. The third UU in the UHIRI ranking is the urban district 6 – Stanga, which is a commercial area with high UHII values as well as a high percentage of foreign residents. It is worth noting that, according to the UHIRI analysis, UUs which are more exposed to heat-related risk are all characterized by high UHII values, since the UHII value is weighted 50% in the UHIRI composition. Unfortunately, due to the different data spatial units (UUs vs postal codes), the UHIRI does not include HLIRI in the spatial analysis; HAERI is also excluded since it is strongly correlated to HERI.

The UHIRI map is presented in Fig. 12: The color of the UUs represents the UHIRI, while the histogram quantifies the contribution of the three vulnerabilities to the UHIRI itself.

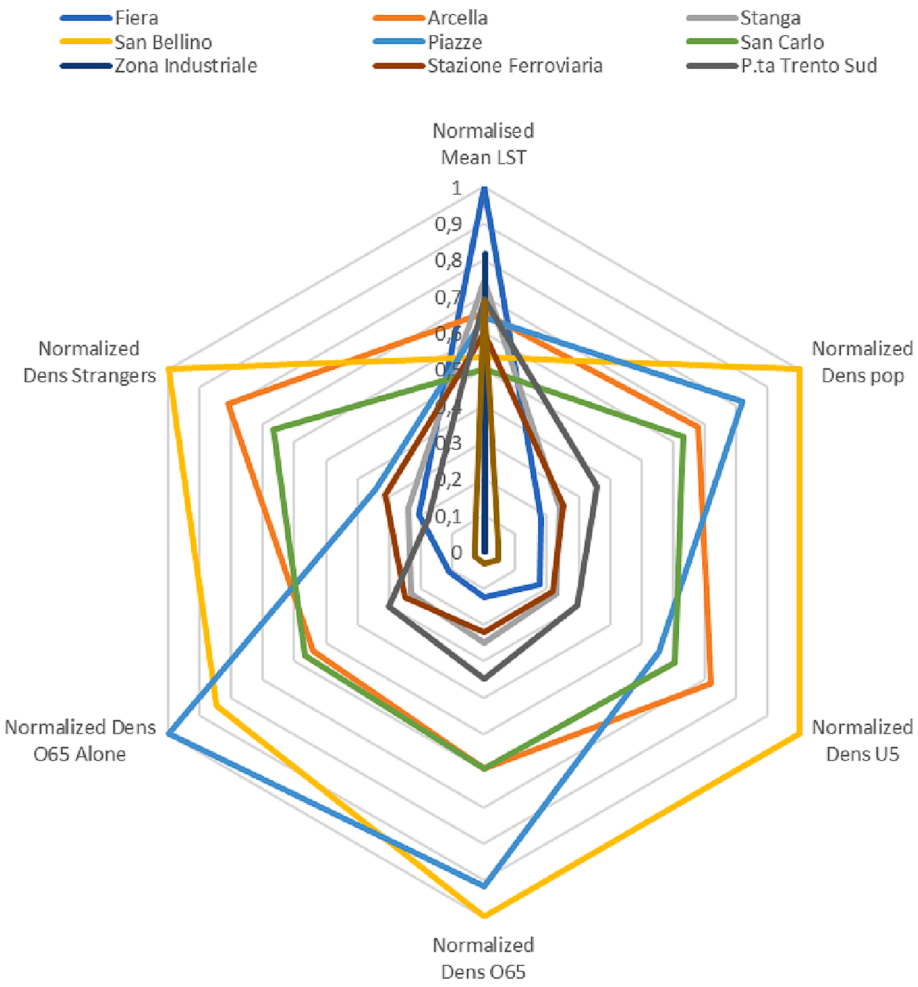

Fig. 13. Radar chart of the 10 Urban Units with the highest UHIRI values and the normalized value of i) mean LST, ii) population density, iii) density of residents under five years old, iv) density of residents over 65 years old, v) density of residents living alone over 65 years old, and vi) density of foreign residents.

To better understand any single contribution in terms of UHII and heat-related vulnerabilities to the global index map we used a radar chart (Fig. 13) to represent the normalized density of vulnerable groups for the 10 UUs with the highest UHIRI values. The chart allows us to identify two groups of UUs among those with the latest UHIRI values which differ in the composition of risk: The first group has higher vulnerability and exposure but less hazard (UUs: San Bellino, Piazze, Arcella, and San Carlo), while the second presents a higher hazard but less vulnerability and exposure (Fiera, Zona Industriale, Stazione, Stanga, and Porta Trento Sud).

3.4. Methodology limitations

This study presents a first GIS-based open-source methodology which include the spatial dimension of some social vulnerabilities to climate change impacts into an integrated UHI climate risk assessment at urban scale. However, it presents some limitations which may affect both the accuracy of UHII assessment and the methodology replicability. Firstly, UHII assessment is based only in LST analyses derived from Landsat 9 images, not considering other meteorological variables based on field observations (air temperature, wind intensity and directions) nor urban features (form and morphology). Moreover, within the calculated HWs time-period only two Landsat image were available. Such limitations do not allow to assess urban microclimate variability at sub-urban nor neighborhood scales. Assessment of spatial and temporal variability of UHI is strongly dependent on the available number of Landsat 8–9 scenes. Availability of night-time Landsat scenes during HWs would also allow to spatially assess UHII at night, highlights possible hotspots for effect on human health of tropical nights. Finally, availability and accuracy of socio-economic spatial data play a crucial role in mapping vulnerable social group to climate risk.

4. Towards just and inclusive climate-resilient adaptation plans

Our findings highlight that the intensity and magnitude of UHIs in the city of Padua are considerable, with temperature anomalies in summer 2022 that might have differed by 5–8 °C from the average values of rural contexts. However, the thermal physical phenomenon is spatially very heterogeneous, with different degrees of UHII distributed over the urban. In fact, UHII is positively correlated with soil sealing in different sectors of the city, especially in the industrial districts, within the train station area, and in the historic city center. The different spatial distribution of sensitive groups might also reflect the socio-cultural and economic dynamics of housing policies in Padua. The climate risk related to UHI is therefore re-shaped according to where these vulnerable groups are concentrated. It is crucial to consider that in some critical UUs the elderly, migrants, children, and low-income households co-exist; thus, risk components can have a cumulative effect (Fig. 12).

Various cities worldwide are progressively designing and developing adaptation plans aiming to reduce UHII and mitigate heat-related discomfort. They are often supported by EU and national policies and strategies, such as the 2013 and 2021 EU strategies on adaptation to climate change. Such strategies are usually based on the incorporation into urban planning of green and blue infrastructures, such as green

areas and water channels, as well as nature-based solutions. More specifically, green infrastructures and nature-based solutions include the use of trees, grass, shrubs, and roofs and walls (Balany et al., 2020). Such urban features perform well in terms of mitigating the thermal intensity of UHI on the urban territory. For example, urban green parks might have significantly lower temperatures than the urbanized surrounding area, with differences of 5 to 12 °C, and their beneficial effects spill over onto surrounding buildings (Lobaccaro & Acero, 2015; Shashua-Bar et al., 2011), while tree cover of at least one third the total surface area might reduce the thermal environment by about 1 °C (Imran et al., 2018). In general, adaptation plans are focused only on the physical environment of the city with no or little regard to the unequal spatial distribution of climate change impact measures (Swanson, 2021). As explained by Mohtat and Khirfan (2021; 2022), mainstream climate adaptation policies "in the absence of power balance checks and political representation, either entrench the political-economic patterns of privilege in allocating adaptive resources or use adaptation as a justification for economic development.".

One of the main aspects of climate justice in urban context is that vulnerability to heat is not equal for all city dwellers. Risk is higher by different degree of exposure (the spatial and temporal dimension of UHII and magnitude), demographic susceptibility (elderly, children, and foreigner residents), socio-economic and cultural factors. Understanding the dimension of "where" and "who" combined is affected by heat-related risk is therefore essential to support inclusive and more just adaptation measures, reinforcing the importance of social inequalities in urban planning for climate change adaptation.

Therefore, it is important to better investigate how the implementation of climate adaptation plans might directly or indirectly affect the vulnerability of disadvantaged urban populations as strategies and regulations might themselves exacerbate, maintain, or ignore present and future inequalities by creating injustice and unequal interventions (Barnett, 2006; Anguelovski et al., 2016).

Based on our findings, we stress that green and blue infrastructures as well as nature-based solutions are currently essential to mitigate the consequences of HWs and UHIs on urban populations, but their implementation in adaptation plans should also respect the spatial dimension of climate justice. Finally, as our understanding of the spatial dimension of social vulnerabilities to climate risk remains limited, the design as well the criteria for urban adaptation plans should be data-driven so as to first identify priorities in terms of intervention areas.

5. Conclusions

Our study frames the issue of climate justice related to extreme meteorological events in urban areas, such as HWs and UHIs. Our GIS-based methodology proposes a replicable and scalable open-access workflow to map UHII and to perform an integrated assessment of climate risk which can include the unequal distribution of both impacts from extreme events and socioeconomic vulnerabilities.

Our findings indicate that, during summer 2022, three extreme HWs hit the urban territory of Padua, increasing the climate risk for vulnerable social groups in six critical sectors of the city. Impervious surfaces amplify UHII by 0.3 °C for every 10% of soil sealing, on average. The integrated heat-related risk analysis highlights that critical areas are characterized by high numbers of the elderly, migrants, children, and low-income households. Given the forecast increase in the magnitude and frequency of extreme HW events in the near future, mitigation actions to protect the health of urban dwellers are urgently required. Nature-based solutions as well as the implementation of green and blue infrastructures are very effective in mitigating UHII; however, climate-resilient policies and strategies should also respect the spatial dimension of climate justice and design more inclusive and just adaptation plans.

Declaration of Competing Interest

The authors declare that they have no known competing financial interests or personal relationships that could have appeared to influence the work reported in this paper.

Data availability

Data will be made available on request.

Acknowledgements

This article is part of the research activities of the Jean Monnet Center of Excellence on Climate Justice, by the support of Erasmus + Programme of the European Union, call for proposals EAC/A02/2019–Jean Monnet Activities; Decision number 620401; Project number: 620401-EPP-1-2020-1-IT-EPPJMO-CoE.

Appendix A. – LST calculation

LST within a 15 km buffer radius from the centroid of the municipality of Padova was calculated from Landsat thermal band (TIRS1). The methodology follows USGS LST guidelines (Zanter, 2018). The calculation of UHII – the difference between background rural and highest urban temperatures (Oke, 1973) – follows the methodology by RUS-Copernicus (Serco Italia SPA, 2018). All LST calculations were performed pixel-by-pixel for each Landsat scene, by using R Studio, a free and open-source statistical software.

From digital numbers to top of atmosphere reflectance and top of atmosphere brightness temperature

Landsat bands downloaded from https://earthexplorer.usgs.gov are GEOTIFF files containing Digital Numbers (DN) as raw data. Calculations for the transformation of DN into Top of Atmosphere Reflectance (TOAR) for bands 4 and 5 (Eq. (5), and Top of Atmosphere Brightness Temperature (TOABT) for thermal band 10 (Eqs. (6) and (7) are provided by Landsat metadata.

$$\rho_{\lambda} = \frac{M_{\rho,i} Q_{cal,i} + A_{\rho,i}}{sinsin(\theta_{SE})} \tag{5}$$

where:

ρ_{λ} = top of atmosphere reflectance.
$M_{\rho,i}$ = multiplicative factor of band.$i = 4,5$
$Q_{cal,i}$ = DN of band.$i = 4,5$
$A_{\rho,i}$ = additive factor of band.$i = 4,5$
θ_{SE} = sun elevation angle in the center of the scene expressed in degrees

$$L_\lambda = M_L Q_{cal} + A_L \tag{6}$$

where:
L_λ = spectral radiance.
M_L = multiplicative factor of band 10.
Q_{cal} = DN of band 10.
A_L = additive factor of band 10

$$BT = \frac{K_2}{lnln\left(\frac{K_1}{L_\lambda} + 1\right)} \tag{7}$$

where:
BT = Top of atmosphere brightness temperature.
K_1 = thermal conversion constant 1 given by Landsat 8 metadata.
K_2 = thermal conversion constant 2 given by Landsat 8 metadata.
L_λ = top of atmosphere spectral radiance.

Calculation of the normalized difference vegetation Index and proportion of vegetation

We calculated the widely adopted Normalized Difference Vegetation Index (NDVI) as defined in Equation (8). NDVI ranges from −1 to 1 providing, by increasing values, different degrees of greenness (Yuan & Bauer, 2007). Moreover, the specific emissivity of the different land cover types is derived from NDVI analysis. From NDVI it is possible to calculate an estimation of proportion of vegetation (Equation (9).

$$NDVI = \frac{NIR - RED}{NIR + RED} \tag{8}$$

where:
$NDVI$ = Net Difference Vegetation Index.
NIR = band 5 reflectance.
RED = band 4 reflectance

$$P_v = \frac{NDVI - NDVI_{min}}{NDVI_{max} - NDVI_{min}} \tag{9}$$

where:
P_v = Proportion of vegetation.
$NDVI$ = Net difference vegetation index.
$NDVI_{max}$ = 0.8.
$NDVI_{min}$ = 0.2.

Emissivity and land surface temperature

The emissivity of the earth surface is the average emissivity of the single elements present within a pixel; it is estimated from the vegetation proportion values defined in Equation (10) (AnandaBabu et al., 2018).

$$e = 0.004 P_v + 0.986 \tag{10}$$

where:
e = emissivity.
P_v = proportion of vegetation.
Finally, LST is estimated from Equation (11).

$$LST = \frac{BT}{1 + [(WBT/\rho) lnln(e)]} \tag{11}$$

where:
LST = land surface temperature.
BT = top of atmosphere brightness temperature.
e = emissivity.
W = average wavelength of band 10 given by Landsat metadata.
$\rho = hc/\sigma$ with σ Boltzmann constant, h Planck constant and c the speed of light.

Appendix B – UUs data

Urban Unit Details					Demography						UHI Intensity				Indexes				
UU ID	UU N°	UU Name	Surface (km2)	Built-up	Pop	Dens. Pop	% Under 5	% Over 65	% Over 65 Alone	% Strangers	Mean	Min	Max	σ	Global UHI Risk Index	HCRI	HERI	HEARI	HSRI
10	5.1	Fiera	1,02	86%	1.981	1.949	4,4	18,7	5,9	30,0	3,40	0,54	7,89	1,61	1,00	1,00	0,79	0,79	1,00
31	25.1	Arcella	2,25	85%	15.971	7.103	4,8	23,4	8,0	32,2	2,09	-1,64	4,24	0,79	0,91	0,97	0,82	0,80	0,96
12	6	Stanga	1,40	71%	3.586	2.554	4,4	27,7	9,6	26,7	2,42	-1,00	5,97	1,47	0,88	0,78	0,81	0,77	0,81
32	25.2	San Bellino	0,34	86%	3.510	10.415	4,6	26,8	8,5	27,0	1,63	-0,88	2,61	0,53	0,86	0,96	0,92	0,85	0,93
1	1.1	Piazze	0,80	93%	6.855	8.566	3,1	29,8	12,2	11,3	2,03	-0,25	3,55	0,78	0,74	0,76	1,00	1,00	0,75
30	24	San Carlo	2,23	72%	14.695	6.604	4,4	25,2	9,0	28,5	1,50	-2,70	4,24	1,00	0,74	0,73	0,73	0,71	0,80
37	30.1	Zona Industriale	8,07	76%	560	69	4,1	18,8	2,7	21,3	2,71	-4,52	8,72	2,13	0,73	0,69	0,59	0,48	0,71
11	5.2	Stazione Ferroviaria	0,83	81%	2.213	2.676	3,9	23,4	9,8	33,0	1,88	-1,24	5,23	1,44	0,73	0,58	0,62	0,68	0,79
8	4.1	P.ta Trento Sud	0,63	91%	2.376	3.789	3,7	25,8	8,4	13,5	2,22	-0,47	3,75	0,65	0,70	0,69	0,78	0,73	0,66
35	28	San Lazzaro	3,44	72%	1.829	532	4,5	19,1	5,8	17,5	2,21	-3,46	6,42	1,71	0,63	0,65	0,52	0,52	0,59
7	3	San Giuseppe	1,24	88%	7.328	5.912	3,4	30,1	11,5	10,3	1,58	-0,18	3,14	0,55	0,61	0,58	0,82	0,80	0,58
40	32	Granze	1,73	52%	845	487	3,9	21,5	5,1	14,0	2,19	-1,66	7,82	1,88	0,59	0,55	0,56	0,49	0,55
2	1.2	Savonarola	1,19	76%	6.451	5.444	3,0	34,2	11,0	11,4	1,35	-0,64	3,98	0,73	0,58	0,44	0,84	0,72	0,53
3	1.3	Santo-Portello	1,63	80%	6.968	4.287	3,1	27,9	10,4	12,9	1,67	-1,69	3,90	1,00	0,57	0,48	0,73	0,72	0,57
36	29	Ponte di Brenta	1,27	59%	3.410	2.680	4,3	29,4	9,3	16,6	1,22	-2,23	3,01	0,86	0,56	0,48	0,61	0,54	0,48
13	7	Forcellini	2,66	58%	9.610	3.613	4,0	29,7	8,7	10,3	1,35	-2,74	4,60	1,06	0,55	0,51	0,68	0,57	0,46
16	10	Voltabarozzo	2,07	49%	5.286	2.556	4,2	23,7	7,5	11,6	1,56	-2,33	4,55	1,05	0,52	0,54	0,56	0,53	0,48
15	9	Madonna Pellegrina	1,08	73%	6.584	6.089	3,9	26,7	9,6	12,2	1,12	-2,14	3,85	1,08	0,52	0,55	0,66	0,65	0,52
29	23	Pontevigodarzere	1,91	47%	5.242	2.741	4,8	23,2	6,6	25,2	0,83	-2,53	3,57	1,23	0,50	0,45	0,41	0,37	0,51
19	13	Guizza	4,25	45%	12.574	2.961	4,4	26,5	8,7	17,2	1,01	-2,94	4,51	1,35	0,49	0,45	0,52	0,49	0,46
4	1.4	Prato della Valle	0,76	79%	3.140	4.132	2,8	32,3	11,3	8,8	1,25	-1,52	3,16	0,88	0,48	0,33	0,74	0,67	0,44
14	8	Sant'Osvaldo	2,23	65%	10.870	4.869	3,5	29,3	10,0	9,9	1,06	-3,11	4,41	1,24	0,47	0,42	0,66	0,61	0,44
22	16	Cave	2,07	58%	4.239	2.045	3,9	25,1	9,3	23,1	0,90	-3,04	7,35	1,57	0,45	0,31	0,44	0,45	0,48
9	4.2	P.ta Trento Nord	0,46	50%	626	1.348	4,0	25,4	8,5	14,4	1,13	-1,21	3,49	1,01	0,43	0,35	0,47	0,45	0,39
21	15	Brusegana	3,57	38%	7.268	2.035	4,7	24,9	8,6	23,2	0,58	-3,62	3,47	1,26	0,43	0,35	0,37	0,37	0,42
6	2	Sacra Famiglia	2,77	44%	7.234	2.607	3,7	29,6	10,4	8,9	0,97	-3,00	4,57	1,40	0,41	0,32	0,57	0,53	0,34
5	1.5	Città Giardino	0,78	77%	4.080	5.260	3,6	30,1	10,6	7,8	0,62	-2,19	3,23	1,19	0,38	0,35	0,61	0,56	0,35
17	11	SS. Crocifisso	2,44	36%	4.686	1.917	4,9	22,1	6,4	8,5	0,84	-3,19	3,47	1,17	0,36	0,43	0,36	0,33	0,29
38	30.2	Is. di Terranegra	1,18	30%	246	209	2,0	35,8	10,6	6,9	1,11	-3,04	7,39	1,46	0,34	0,00	0,64	0,48	0,26
33	26	Mortise	1,89	47%	6.343	3.353	1,8	29,6	9,7	18,5	0,78	-3,10	3,79	1,33	0,33	0,02	0,56	0,49	0,45
39	31	Camin	2,25	38%	3.916	1.740	3,9	20,9	5,2	16,0	0,83	-2,32	5,65	1,57	0,32	0,27	0,32	0,28	0,37
20	14	Mandria	8,92	28%	10.076	1.130	3,4	27,9	6,0	9,4	0,76	-3,37	5,23	1,52	0,30	0,17	0,44	0,28	0,26
23	17	Vrentelle	2,60	36%	4.222	1.625	4,2	27,4	6,8	18,3	0,20	-3,72	4,92	1,71	0,30	0,16	0,33	0,22	0,28
34	27	Torre	3,07	37%	4.502	1.468	3,2	25,0	6,2	12,3	0,75	-3,60	4,87	1,38	0,28	0,14	0,39	0,30	0,30
24	18	Sanr'Ignazio	1,37	42%	3.724	2.726	3,7	21,2	6,1	8,5	0,70	-3,19	3,07	1,29	0,26	0,26	0,34	0,32	0,29
28	22	Altichiero	3,54	34%	4.197	1.187	4,2	22,9	6,0	8,5	0,59	-4,80	4,01	1,35	0,26	0,24	0,30	0,25	0,22
18	12	Salboro	4,71	19%	2.531	538	3,2	23,0	5,4	4,0	1,03	-3,12	6,26	1,52	0,24	0,16	0,36	0,28	0,23
27	21	Sacro Cuore	4,96	30%	4.882	985	3,8	24,1	6,7	16,4	0,16	-4,15	4,85	1,66	0,20	0,07	0,23	0,19	0,23
26	20	Ponterotto	2,82	25%	2.647	940	4,3	18,3	4,5	8,4	-0,04	-3,33	3,47	1,46	0,06	0,08	0,07	0,07	0,10
25	19	Montà	0,91	26%	1.197	1.311	4,9	17,9	4,3	4,4	-0,41	-3,71	3,20	1,49	0,00	0,11	0,00	0,00	0,00

Appendix C – Vulnerability maps

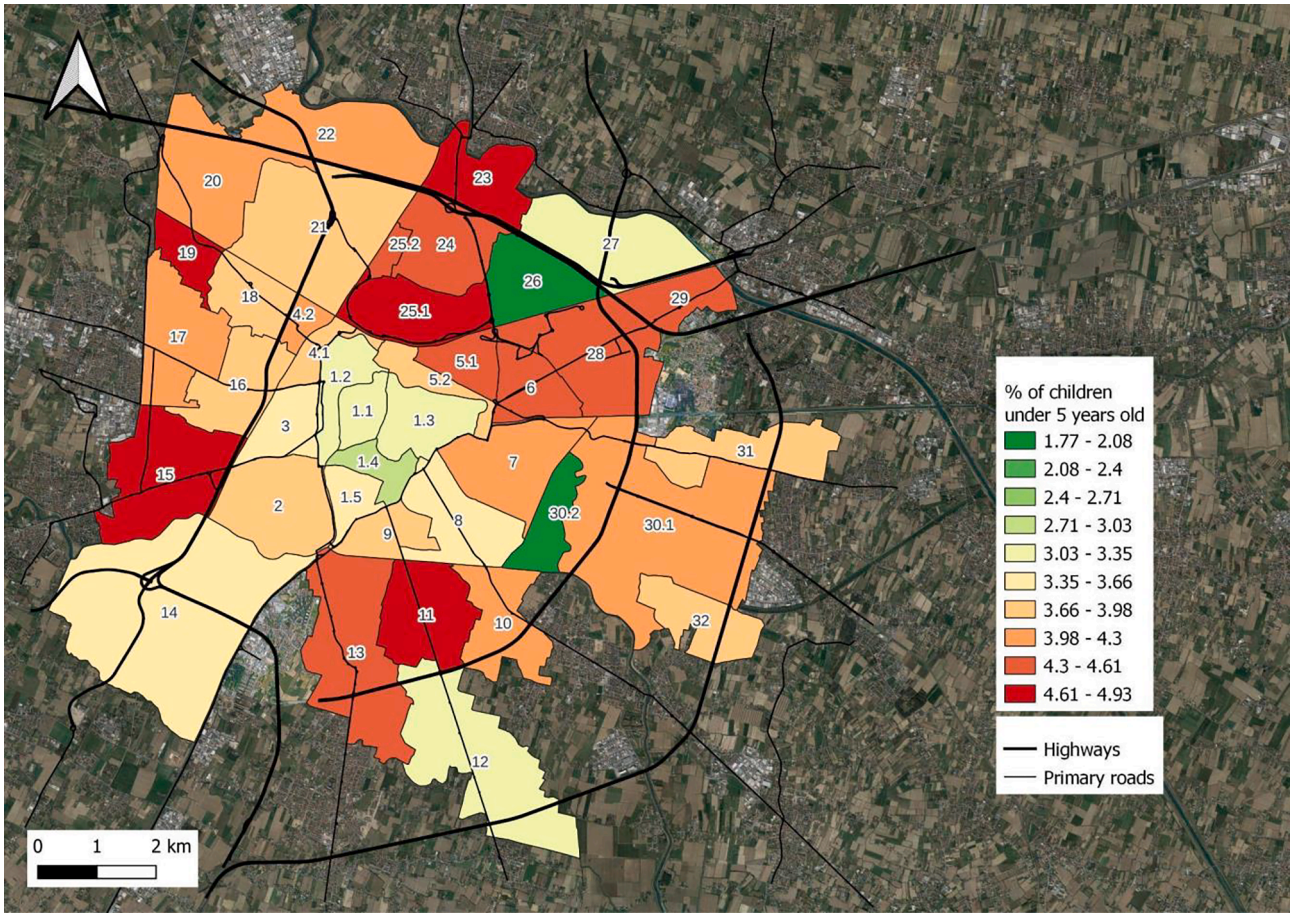

Fig. A1. % of children under 5 years old in UUs.

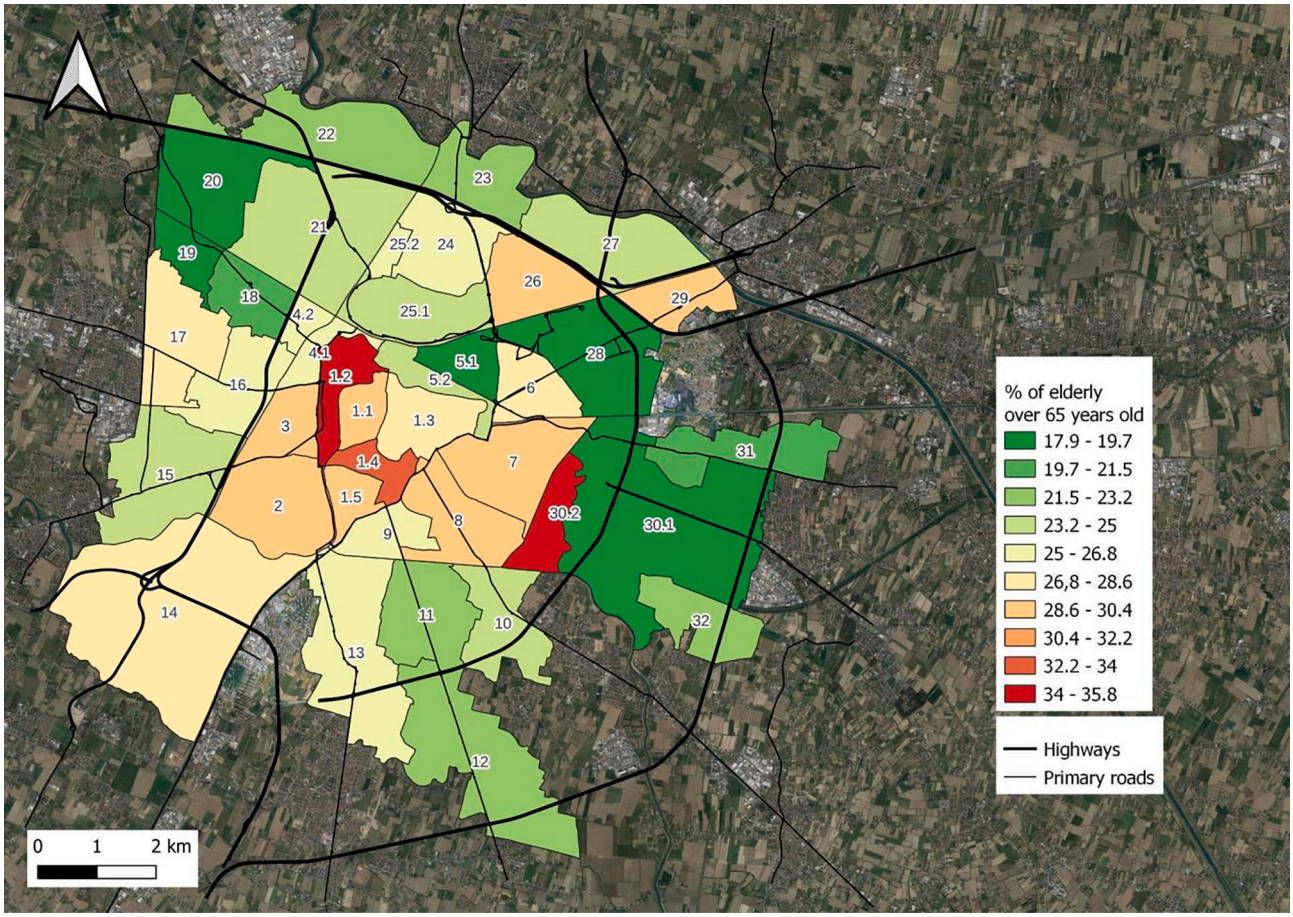

Fig. A2. % of elderly over 65 years old in UUs.

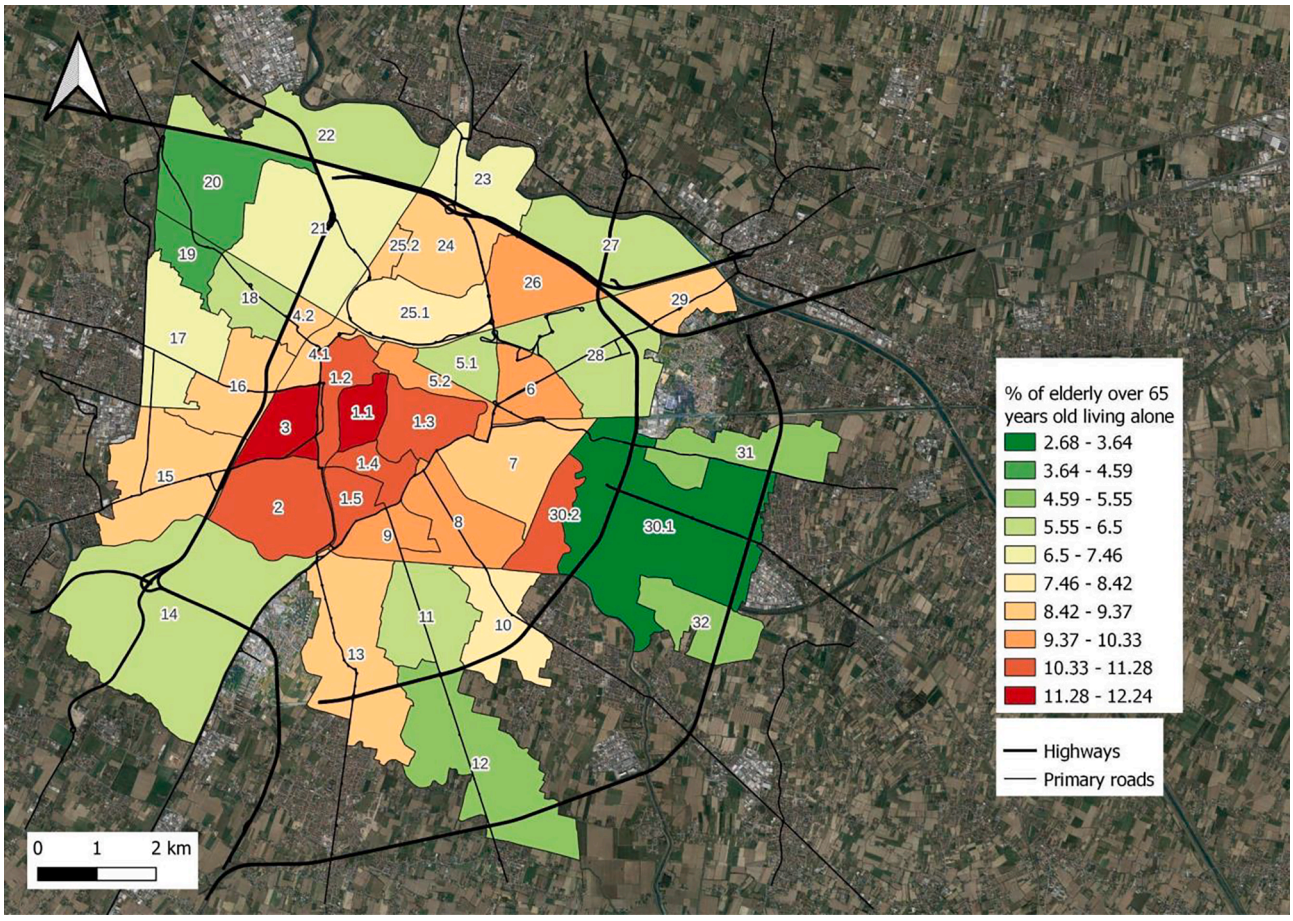

Fig. A3. % of elderly over 65 years old living alone in UUs.

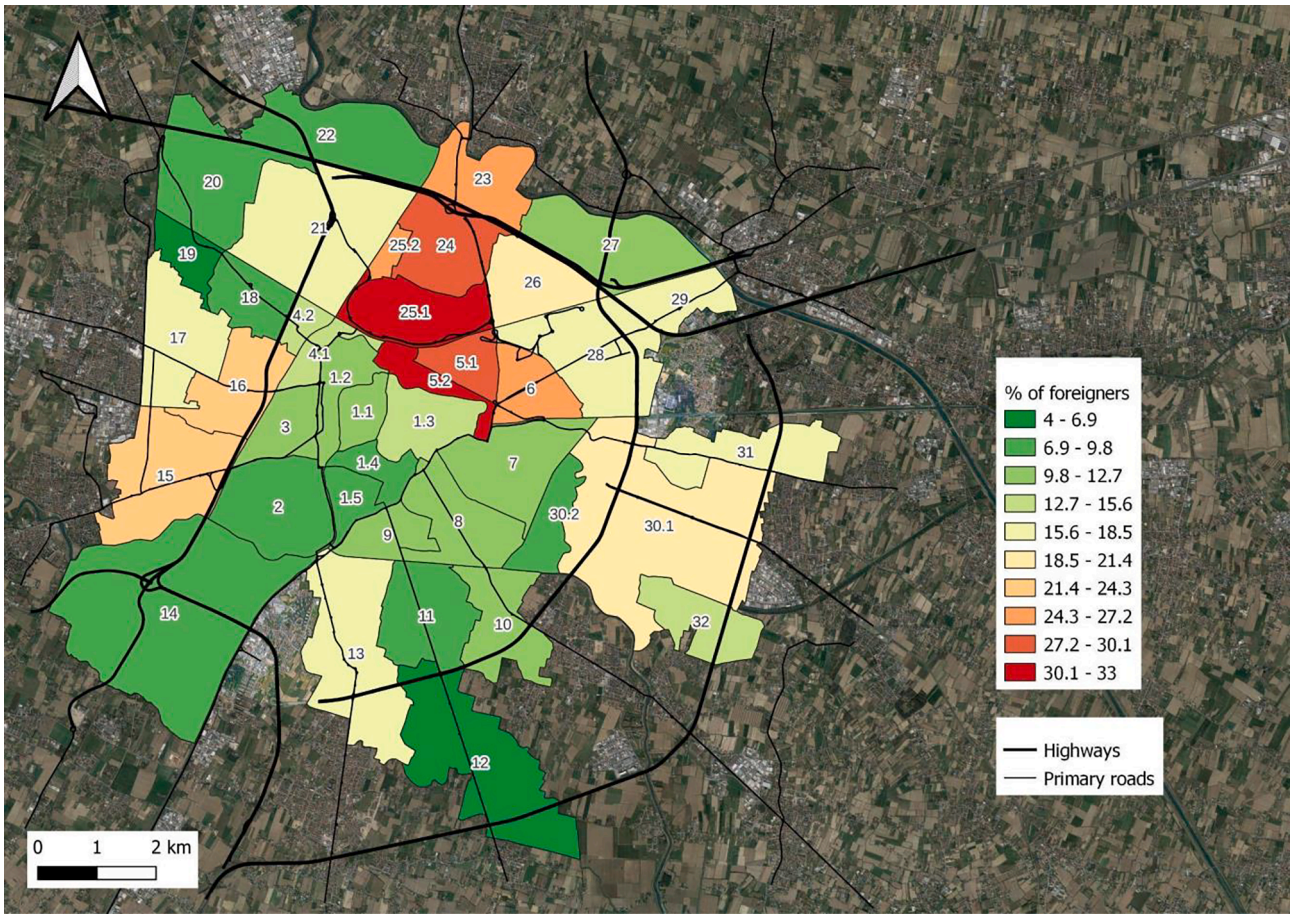

Fig. A4. % of foreigners in UUs.

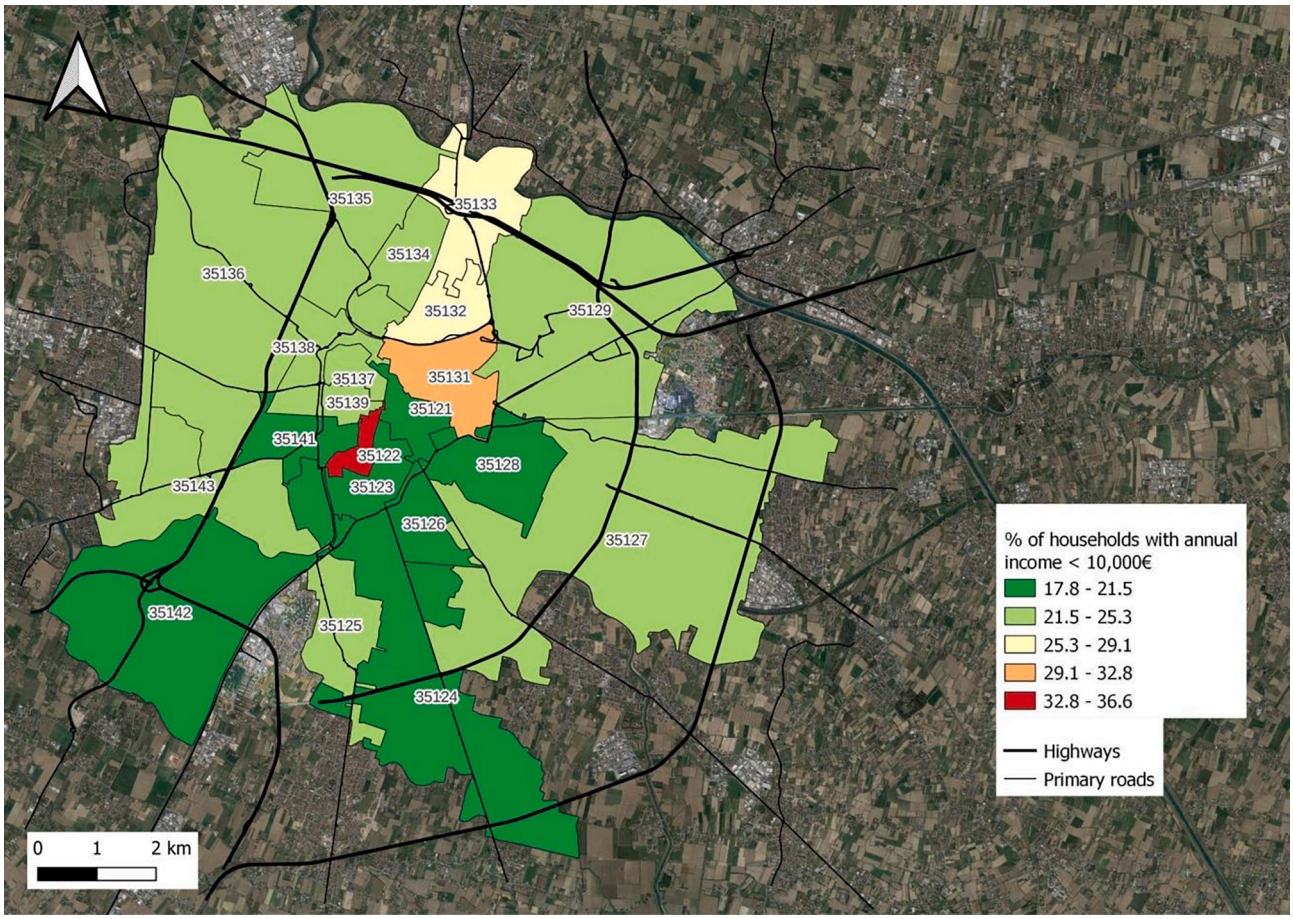

Fig. A5. % of households with annual income <10,000 in UUs.

References

Amado, C. (2022). *Unravelling the Urban Heat Island Phenomenon in the Netherlands. A Multicity Spatial Analysis on the Distributive component of Environmental Justice, analysing the Urban Green Infrastructure, and the Urban Heat Island Effect. A Multicity Spatial Analysis on the Distributive component of Environmental Justice, analysing the Urban Green Infrastructure, and the Urban Heat Island Effect* (January 12, 2022).

AnandaBabu, D., PurushothamanB, M., & Babu, S. S. (2018). Estimation of land surface temperature using LANDSAT 8 data. *International Journal of Advance Research, Ideas and Innovations in Technology, 4*.

Andersson J., & Faulkner D. (2022, July 19). Heatwave: Fires blaze after UK passes 40C for first time. *BBC*. https://www.bbc.com/news/uk-62217282 (accessed 5 January 2023).

Anguelovski, I., Shi, L., Chu, E., Gallagher, D., Goh, K., Lamb, Z., … Teicher, H. (2016). Equity impacts of urban land use planning for climate adaptation: Critical perspectives from the global north and south. *Journal of Planning Education and Research, 36*(3), 333–348.

ARPAV. (2022). HWF - Giorni di ondata di calore accessed 5 January 2023 https://www.arpa.veneto.it/arpavinforma/indicatori-ambientali/indicatori_ambientali/clima-e-rischi-naturali/clima/hwf-giorni-di-ondata-di-calore/2021.

Arsad, F. S., Hod, R., Ahmad, N., Ismail, R., Mohamed, N., Baharom, M., … Tangang, F. (2022). The impact of heatwaves on mortality and morbidity and the associated vulnerability factors: A systematic review. *International Journal of Environmental Research and Public Health, 19*(23), 16356.

Åström, D. O., Bertil, F., & Joacim, R. (2011). Heat wave impact on morbidity and mortality in the elderly population: A review of recent studies. *Maturitas, 69*(2), 99–105.

Balany, F., Ng, A. W., Muttil, N., Muthukumaran, S., & Wong, M. S. (2020). Green infrastructure as an urban heat island mitigation strategy—A review. *Water, 12*(12), 3577.

Barnett, J. (2006). *Climate change, insecurity, and injustice* (pp. 115–130). Cambridge, MA, USA: MIT Press.

Busato, F., Lazzarin, R. M., & Noro, M. (2014). Three years of study of the Urban Heat Island in Padua: Experimental results. *Sustainable Cities and Society, 10*, 251–258.

Churchill, S. A., & Smyth, R. (2021). Energy poverty and health: Panel data evidence from Australia. *Energy Economics, 97*, 105219.

Ciais, P., Reichstein, M., Viovy, N., Granier, A., Ogée, J., Allard, V., … Valentini, R. (2005). Europe-wide reduction in primary productivity caused by the heat and drought in 2003. *Nature, 437*(7058), 529–533.

Colelli, F. P., Emmerling, J., Marangoni, G., Mistry, M. N., & De Cian, E. (2022). Increased energy use for adaptation significantly impacts mitigation pathways. *Nature Communications, 13*(1), 4964.

Comune di Padova. (2022). Annuario Statistico 2021 accessed 5 January 2023 https://www.padovanet.it/informazione/padova-cifre.

Conti, S., Masocco, M., Meli, P., Minelli, G., Palummeri, E., Solimini, R., … Vichi, M. (2007). General and specific mortality among the elderly during the 2003 heat wave in Genoa (Italy). *Environmental Research, 103*(2), 267–274.

Dosio, A., Mentaschi, L., Fischer, E. M., & Wyser, K. (2018). Extreme heat waves under 1.5 C and 2 C global warming. *Environmental Research Letters, 13*(5), 054006.

Du, H., Wang, D., Wang, Y., Zhao, X., Qin, F., Jiang, H., & Cai, Y. (2016). Influences of land cover types, meteorological conditions, anthropogenic heat and urban area on surface urban heat island in the Yangtze River Delta Urban Agglomeration. *Science of the Total Environment, 571*, 461–470.

Espírito Santo, F., de Lima, M. I. P., Ramos, A. M., & Trigo, R. M. (2014). Trends in seasonal surface air temperature in mainland Portugal, since 1941. *International Journal of Climatology, 34*(6), 1814–1837.

Eurostat. (2022). Excess mortality hits +16%, highest 2022 value so far. https://ec.europa.eu/eurostat/en/web/products-eurostat-news/-/ddn-20220916-1.

Fears D., & Eger A. (2022, July 19). As heat waves hit U.S. and Europe, leaders split on climate change. *The Washington Post*. https://www.washingtonpost.com/climate-environment/2022/07/19/heat-wave-europe-climate-change/ (accessed 5 January 2023).

Founda, D., & Santamouris, M. (2017). Synergies between Urban Heat Island and Heat Waves in Athens (Greece), during an extremely hot summer (2012). *Scientific Reports, 7*(1), 1–11.

Gardiner, S. M. (2011). *A perfect moral storm: The ethical tragedy of climate change*. Oxford University Press.

Ge, X., Mauree, D., Castello, R., & Scartezzini, J. L. (2020). Spatio-temporal relationship between land cover and land surface temperature in urban areas: A case study in Geneva and Paris. *ISPRS International Journal of Geo-Information, 9*(10), 593.

Gualtieri A. E., & Sundby A. (2022, July 23). Heat waves are hitting around the globe. Scientists say climate change is making them more frequent. *CBS News*. https://

www.cbsnews.com/news/heat-wave-climate-change-getting-more-frequent/ (accessed 5 January 2023).
Guerreiro, S. B., Dawson, R. J., Kilsby, C., Lewis, E., & Ford, A. (2018). Future heat-waves, droughts and floods in 571 European cities. *Environmental Research Letters, 13*(3), 034009.
He, B. J., Zhao, D., Dong, X., Xiong, K., Feng, C., Qi, Q., … Pathak, M. (2022). Perception, physiological and psychological impacts, adaptive awareness and knowledge, and climate justice under urban heat: A study in extremely hot-humid Chongqing, China. *Sustainable Cities and Society, 79*, 103685.
Imran, H. M., Kala, J., Ng, A. W. M., & Muthukumaran, S. (2018). Effectiveness of green and cool roofs in mitigating urban heat island effects during a heatwave event in the city of Melbourne in southeast Australia. *Journal of Cleaner Production, 197*, 393–405.
IPCC. (2021). Climate Change 2021: The Physical Science Basis. Contribution of Working Group I to the Sixth Assessment Report of the Intergovernmental Panel on Climate Change [Masson-Delmotte, V., P. Zhai, A. Pirani, S.L. Connors, C. Péan, S. Berger, N. Caud, Y. Chen, L. Goldfarb, M.I. Gomis, M. Huang, K. Leitzell, E. Lonnoy, J.B.R. Matthews, T.K. Maycock, T. Waterfield, O. Yelekçi, R. Yu, and B. Zhou (eds.)]. Cambridge University Press, Cambridge, United Kingdom and New York, NY, USA, 2391 pp. doi:10.1017/9781009157896.
IPCC. (2022). Summary for Policymakers [H.-O. Pörtner, D.C. Roberts, E.S. Poloczanska, K. Mintenbeck, M. Tignor, A. Alegría, M. Craig, S. Langsdorf, S. Löschke, V. Möller, A. Okem (eds.)]. In: Climate Change 2022: Impacts, Adaptation and Vulnerability. Contribution of Working Group II to the Sixth Assessment Report of the Intergovernmental Panel on Climate Change [H.-O. Pörtner, D.C. Roberts, M. Tignor, E.S. Poloczanska, K. Mintenbeck, A. Alegría, M. Craig, S. Langsdorf, S. Löschke, V. Möller, A. Okem, B. Rama (eds.)]. Cambridge University Press, Cambridge, UK and New York, NY, USA, pp. 3–33, doi:10.1017/9781009325844.001.
Javanroodi, K., Nik, V. M., & Scartezzini, J. L. (2021, November). Quantifying the impacts of urban morphology on modifying microclimate conditions in extreme weather conditions. In *Journal of Physics: Conference Series* (Vol. 2042, No. 1, p. 012058). IOP Publishing.
Javanroodi, K., Nik, V. M., Giometto, M. G., & Scartezzini, J. L. (2022). Combining computational fluid dynamics and neural networks to characterize microclimate extremes: Learning the complex interactions between meso-climate and urban morphology. *Science of The Total Environment, 829*, 154223.
Kotharkar, R., & Surawar, M. (2016). Land use, land cover, and population density impact on the formation of canopy urban heat islands through traverse survey in the Nagpur urban area, India. *Journal of Urban Planning and Development, 142*(1), 04015003.
Kovats, R. S., Hajat, S., & Wilkinson, P. (2004). Contrasting patterns of mortality and hospital admissions during hot weather and heat waves in Greater London, UK. *Occupational and Environmental Medicine, 61*(11), 893–898.
Liao, W., Hong, T., & Heo, Y. (2021). The effect of spatial heterogeneity in urban morphology on surface urban heat islands. *Energy and Buildings, 244*, 111027.
Lobaccaro, G., & Acero, J. A. (2015). Comparative analysis of green actions to improve outdoor thermal comfort inside typical urban street canyons. *Urban Climate, 14*, 251–267.
Matthies, F., & Menne, B. (2009). Prevention and management of health hazards related to heatwaves. *International Journal of Circumpolar Health, 68*(1), 8–12.
Mentaschi, L., Duveiller, G., Zulian, G., Corbane, C., Pesaresi, M., Maes, J., … Feyen, L. (2022). Global long-term mapping of surface temperature shows intensified intra-city urban heat island extremes. *Global Environmental Change, 72*, 102441.
Messeri, A., Morabito, M., Bonafede, M., Bugani, M., Levi, M., Baldasseroni, A., … Marinaccio, A. (2019). Heat stress perception among native and migrant workers in Italian industries—Case studies from the construction and agricultural sectors. *International Journal of Environmental Research and Public Health, 16*(7), 1090.
Mitchell, B. C., Chakraborty, J., & Basu, P. (2021). Social inequities in urban heat and greenspace: Analyzing Climate Justice in Delhi, India. *International Journal of Environmental Research and Public Health, 18*(9), 4800.
Mitchell, D., Heaviside, C., Vardoulakis, S., Huntingford, C., Masato, G., Guillod, B. P., … Allen, M. (2016). Attributing human mortality during extreme heat waves to anthropogenic climate change. *Environmental Research Letters, 11*(7), 074006.
Mohtat, N., & Khirfan, L. (2021). The climate justice pillars vis-à-vis urban form adaptation to climate change: A review. *Urban Climate, 39*, 100951.
Mohtat, N., & Khirfan, L. (2022). Distributive justice and urban form adaptation to flooding risks: Spatial analysis to identify Toronto's priority neighborhoods. *Frontiers in Sustainable Cities, 4*, 919724.
Morabito, M., Crisci, A., Gioli, B., Gualtieri, G., Toscano, P., Di Stefano, V., … Gensini, G. F. (2015). Urban-hazard risk analysis: Mapping of heat-related risks in the elderly in major Italian cities. *PLoS one, 10*(5), e0127277.
Munafò, M. (2022). *Consumo di suolo, dinamiche territoriali e servizi ecosistemici. Edizione 2022*. Report SNPA 32/22.
Naumann, G., Russo, S., Formetta, G., Ibarreta, D., Forzieri, G., Girardello, M., & Feyen, L. (2020). Global warming and human impacts of heat and cold extremes in the EU. *JRC PESETA IV Project—Task, 11*.
Nayak, S. G., Shrestha, S., Kinney, P. L., Ross, Z., Sheridan, S. C., Pantea, C. I., … Hwang, S. A. (2018). Development of a heat vulnerability index for New York State. *Public Health, 161*, 127–137.
Nitschke, M., Tucker, G. R., Hansen, A. L., Williams, S., Zhang, Y., & Bi, P. (2011). Impact of two recent extreme heat episodes on morbidity and mortality in Adelaide, South Australia: A case-series analysis. *Environmental Health, 10*(1), 1–9.
Noro, M., Busato, F., & Lazzarin, R. M. (2015). Urban heat island in Padua, Italy: Experimental and theoretical analysis. *Indoor and Built Environment, 24*(4), 514–533.
Obradovich, N., Migliorini, R., Paulus, M. P., & Rahwan, I. (2018). Empirical evidence of mental health risks posed by climate change. *Proceedings of the National Academy of Sciences, 115*(43), 10953–10958.
Oke, T. R. (1973). City size and the urban heat island. *Atmospheric Environment (1967), 7*(8), 769-779.
Otto, I. M., Reckien, D., Reyer, C. P., Marcus, R., Le Masson, V., Jones, L., … Serdeczny, O. (2017). Social vulnerability to climate change: A review of concepts and evidence. *Regional Environmental Change, 17*(6), 1651–1662.
Palinkas, L. A., & Wong, M. (2020). Global climate change and mental health. *Current Opinion in Psychology, 32*, 12–16.
Paravantis, J., Santamouris, M., Cartalis, C., Efthymiou, C., & Kontoulis, N. (2017). Mortality associated with high ambient temperatures, heatwaves, and the urban heat island in Athens, Greece. *Sustainability, 9*(4), 606.
Peng, W., Wang, R., Duan, J., Gao, W., & Fan, Z. (2022). Surface and canopy urban heat islands: Does urban morphology result in the spatiotemporal differences? *Urban Climate, 42*, 101136.
Peroni, F., Pappalardo, S. E., Facchinelli, F., Crescini, E., Munafò, M., Hodgson, M. E., & De Marchi, M. (2022). How to map soil sealing, land take and impervious surfaces? A systematic review. *Environmental Research Letters, 17*(5), 053005.
Peroni, F., Pristeri, G., Codato, D., Pappalardo, S. E., & De Marchi, M. (2019). Biotope area factor: An ecological urban index to geovisualize soil sealing in Padua, Italy. *Sustainability, 12*(1), 150.
Phelan, P. E., Kaloush, K., Miner, M., Golden, J., Phelan, B., Silva, H., III, & Taylor, R. A. (2015). Urban heat island: Mechanisms, implications, and possible remedies. *Annual Review of Environment and Resources, 40*, 285–307.
Porfiriev, B. (2014). Evaluation of human losses from disasters: The case of the 2010 heat waves and forest fires in Russia. *International Journal of Disaster Risk Reduction, 7*, 91–99.
Pristeri, G., Peroni, F., Pappalardo, S. E., Codato, D., Castaldo, A. G., Masi, A., & De Marchi, M. (2020). Mapping and assessing soil sealing in Padua municipality through biotope area factor index. *Sustainability, 12*(12), 5167.
Pristeri, G., Peroni, F., Pappalardo, S. E., Codato, D., Masi, A., & De Marchi, M. (2021). Whose urban green? mapping and classifying public and private green spaces in Padua for spatial planning policies. *ISPRS International Journal of Geo-Information, 10*(8), 538.
Robine, J. M., Cheung, S. L. K., Le Roy, S., Van Oyen, H., Griffiths, C., Michel, J. P., & Herrmann, F. R. (2008). Death toll exceeded 70,000 in Europe during the summer of 2003. *Comptes rendus biologies, 331*(2), 171–178.
Romanello, M., McGushin, A., Di Napoli, C., Drummond, P., Hughes, N., Jamart, L., … Hamilton, I. (2021). The 2021 report of the Lancet Countdown on health and climate change: Code red for a healthy future. *The Lancet, 398*(10311), 1619–1662.
Rousi, E., Kornhuber, K., Beobide-Arsuaga, G., Luo, F., & Coumou, D. (2022). Accelerated western European heatwave trends linked to more-persistent double jets over Eurasia. *Nature Communications, 13*(1), 1–11.
Royé, D., Sera, F., Tobías, A., Lowe, R., Gasparrini, A., Pascal, M., … Teixeira, J. P. (2021). Effects of hot nights on mortality in southern Europe. *Epidemiology, 32*(4), 487–498.
Russo, S., Sillmann, J., & Fischer, E. M. (2015). Top ten European heatwaves since 1950 and their occurrence in the coming decades. *Environmental Research Letters, 10*(12), 124003.
Ruuhela, R., Votsis, A., Kukkonen, J., Jylhä, K., Kankaanpää, S., & Perrels, A. (2020). Temperature-related mortality in Helsinki compared to its surrounding region over two decades, with special emphasis on intensive heatwaves. *Atmosphere, 12*(1), 46.
Sakka, A., Santamouris, M., Livada, I., Nicol, F., & Wilson, M. (2012). On the thermal performance of low income housing during heat waves. *Energy and Buildings, 49*, 69–77.
Sanchez-Guevara, C., Peiró, M. N., Taylor, J., Mavrogianni, A., & González, J. N. (2019). Assessing population vulnerability towards summer energy poverty: Case studies of Madrid and London. *Energy and Buildings, 190*, 132–143.
Sangiorgio, V., Fiorito, F., & Santamouris, M. (2020). Development of a holistic urban heat island evaluation methodology. *Scientific Reports, 10*(1), 1–13.
Serco Italia SPA. (2018). Urban heat island with Sentinel-3. (version 1.1) Retrieved from RUS Lectures at https://rus-copernicus.eu/portal/the-rus-library/learn-by-yourself/.
Shashua-Bar, L., Pearlmutter, D., & Erell, E. (2011). The influence of trees and grass on outdoor thermal comfort in a hot-arid environment. *International Journal of Climatology, 31*(10), 1498–1506.
Singh, N., Singh, S., & Mall, R. K. (2020). Chapter 17 - Urban ecology and human health: implications of urban heat island, air pollution and climate change nexus. In P. Verma, P. Singh, R. Singh, & A. S. Raghubanshi (Eds.), *Urban Ecology* (pp. 317–334). doi:10.1016/B978-0-12-820730-7.00017-3.
Stone, B., Jr, Mallen, E., Rajput, M., Gronlund, C. J., Broadbent, A. M., Krayenhoff, E. S., … Georgescu, M. (2021). Compound climate and infrastructure events: How electrical grid failure alters heat wave risk. *Environmental Science & Technology, 55*(10), 6957–6964.
Sultana, F. (2022). Critical climate justice. *The Geographical Journal, 188*(1), 118–124.
Swanson, K. (2021). Equity in urban climate change adaptation planning: A review of research.
Todeschi, V., Pappalardo, S. E., Zanetti, C., Peroni, F., & Marchi, M. D. (2022). Climate justice in the city: Mapping heat-related risk for climate change mitigation of the urban and Peri-Urban Area of Padua (Italy). *ISPRS International Journal of Geo-Information, 11*(9), 490.
Tomlinson, C. J., Chapman, L., Thornes, J. E., & Baker, C. J. (2011). Including the urban heat island in spatial heat health risk assessment strategies: A case study for Birmingham, UK. *International Journal of Health Geographics, 10*(1), 1–14.
UNFCCC. (2021). Report of the Conference of the Parties serving as the meeting of the Parties to the Paris Agreement on its third session, held in Glasgow from 31 October

to 13 November 2021. *United Nations Framework Convention on Climate Change process*; https://unfccc.int/sites/default/files/resource/cma2021_10_add1_adv.pdf (accessed 5 January 2023).

Vandentorren, S., Bretin, P., Zeghnoun, A., Mandereau-Bruno, L., Croisier, A., Cochet, C., … Ledrans, M. (2006). August 2003 heat wave in France: Risk factors for death of elderly people living at home. *The European Journal of Public Health, 16*(6), 583–591.

Vanos, J. K. (2015). Children's health and vulnerability in outdoor microclimates: A comprehensive review. *Environment International, 76*, 1–15.

Wang, J., Xiang, Z., Wang, W., Chang, W., & Wang, Y. (2021). Impacts of strengthened warming by urban heat island on carbon sequestration of urban ecosystems in a subtropical city of China. *Urban Ecosystems, 24*, 1165–1177.

WMO. (2022a, March 17). *Climate change and extreme weather* [Press release]. https://public.wmo.int/en/resources/world-meteorological-day/world-meteorological-day-2022-early-warning-early-action/climate-change-and-extreme-weather (accessed 5 January 2023).

WMO. (2022b, May 18). *Four key climate change indicators break records in 2021* [Press release]. https://public.wmo.int/en/media/press-release/four-key-climate-change-indicators-break-records-2021 (accessed 5 January 2023).

WMO. (2022c, July 29). *"This heatwave is the new normal," says WMO Secretary-General* [Press release https://public.wmo.int/en/media/news/%E2%80%9C-heatwave-new-normal%E2%80%9D-says-wmo-secretary-general (accessed 5 January 2023).

WMO. (2022d, November 25). *Provisional State of the Global Climate in 2022* [Press release]. https://public.wmo.int/en/our-mandate/climate/wmo-statement-state-of-global-climate (accessed 5 January 2023).

World Bank. (2023). Population, total accessed 5 January 2023 https://data.worldbank.org/indicator/SP.POP.TOTL.

Xu, Z., Sheffield, P. E., Su, H., Wang, X., Bi, Y., & Tong, S. (2014). The impact of heat waves on children's health: A systematic review. *International Journal of Biometeorology, 58*, 239–247.

Yensukho, P., Sugsaisakon, S., & Kittipongvises, S. (2022). City-wide greenhouse gas emissions of communities nearby the world heritage site of Ayutthaya, Thailand. *Scientific Reports, 12*(1), 1–11.

Yuan, F., & Bauer, M. E. (2007). Comparison of impervious surface area and normalized difference vegetation index as indicators of surface urban heat island effects in Landsat imagery. *Remote Sensing of environment, 106*(3), 375–386.

Yue, W., Liu, X., Zhou, Y., & Liu, Y. (2019). Impacts of urban configuration on urban heat island: An empirical study in China mega-cities. *Science of the Total Environment, 671*, 1036–1046.

Zanter, K. (2018). *Landsat surface temperature (ST) product guide*. US Geological Survey, Sioux Falls, SD: Department of the Interior. https://www.usgs.gov/media/files/landsat-provisional-surface-temperature-product-guide.